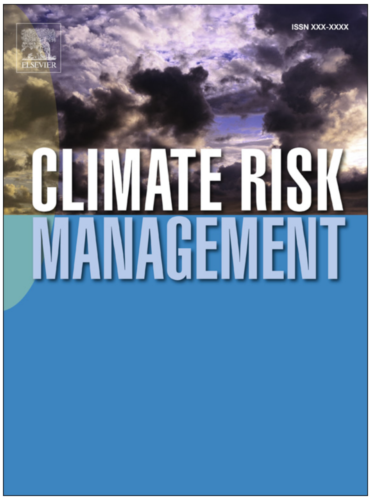

21st Century Flood Risk Projections at Select Sites for the U.S. National Park Service

Peter Van Dusen, Balaji Rajagopalan, David J. Lawrence, Laura Condon, Gary Smillie, Subhrendu Gangopadhyay, Tom Pruitt

PII: S2212-0963(20)30001-2
DOI: https://doi.org/10.1016/j.crm.2020.100211
Reference: CRM 100211

To appear in: *Climate Risk Management*

Received Date: 17 March 2019
Revised Date: 2 December 2019
Accepted Date: 13 January 2020

Please cite this article as: P. Van Dusen, B. Rajagopalan, D.J. Lawrence, L. Condon, G. Smillie, S. Gangopadhyay, T. Pruitt, 21st Century Flood Risk Projections at Select Sites for the U.S. National Park Service, *Climate Risk Management* (2020), doi: https://doi.org/10.1016/j.crm.2020.100211

21st Century Flood Risk Projections at Select Sites for the U.S. National Park Service

Peter Van Dusen[a], Balaji Rajagopalan[a,b], David J. Lawrence[c], Laura Condon[d], Gary Smillie[e], Subhrendu Gangopadhyay[f], and Tom Pruitt[f]

[a]Department of Civil, Environmental and Architectural Engineering, University of Colorado, Boulder, CO, [b]CIRES, University of Colorado, Boulder, CO, [c] Climate Change Response Program, National Park Service, Fort Collins, CO, [d]Department of Hydrology and Atmospheric Sciences, University of Arizona, Tucson, AZ, [e]Water Resources Division, National Park Service, Fort Collins, CO, [f] Bureau of Reclamation, Denver, CO

Abstract

Flood risk studies using stationary flood frequency analysis techniques is commonplace. However, it is increasingly evident that the stationarity assumption of these analyses does not hold as anthropogenic climate change could shift a site's hydroclimate beyond the range of historical behaviors. We employ nonstationary flood frequency models using the generalized extreme value (GEV) distribution to model changing flood risk for select seasons at twelve National Parks across the U.S. In this GEV model, the location and/or scale parameters of the distribution are allowed to change as a function of time-variable covariates. We use historical precipitation and modeled flows from the Variable Infiltration Capacity model (VIC), a land-surface model that simulates land-atmosphere fluxes using water and energy balance equations, as covariates to fit a best nonstationary GEV model to each site. We apply climate model projections of precipitation and VIC flows to these models to obtain future flood frequency estimates. Our model results project a decrease in flood risk for sites in the southwestern U.S. region and an increase in flood risk for sites in northern and eastern regions of the U.S. for the selected seasons. The methods and results presented will enable the NPS to develop strategies to ensure public safety and efficient infrastructure management and planning in a nonstationary climate.

Declarations of Interest: *none*

1. Introduction

Anthropogenic climate change has increased global mean annual land-surface air temperatures and evidence supports a change in the behavior of precipitation (Hartmann et al. 2013) and streamflow extremes (Hirsch and Ryberg 2012; Mallakpour and Villarini 2015; Ahn and Palmer 2016). Given the non-stationary nature of our climate system at present, the common assumption in traditional flood frequency analysis techniques that flood risk will remain stationary into the future must be questioned - climate change is anticipated to continue to shift hydroclimate beyond the range of historical behaviors (Milly et al. 2008).

As temperatures rise, we expect an increase in total precipitable water in the atmosphere (Trenberth et al. 2003), which was already observed over much of North America (Ross and Elliott 1996). Consequently, Hartmann et al. (2013) suggest a likely observed increase in either the frequency or intensity of heavy precipitation events across North America, particularly in central North America. Studies using extreme value theory and precipitation-temperature scaling also generally support this claim (DeGaetano 2009; Wasko and Sharma 2017).

However, trends in observed extreme streamflow are more variable (Ahn and Palmer 2016). Lins and Slack (1999) found both increasing and decreasing trends in historical streamflow extremes in the eastern U.S. with a general decrease in extremes in western U.S., the Pacific Northwest, and the Southern Plains. Mallakpour and Villarini (2015) found an increase in the frequency of observed floods in the central U.S., with no evidence to support a change in the observed magnitude of flood events. In the southwestern U.S., Hirsch and Ryberg (2012) found decreasing flood magnitudes associated with increasing atmospheric greenhouse gas (GHG) levels, while the eastern and northeastern U.S. showed increasing, but non-significant, flood magnitude trends in response to carbon dioxide increases.

Flood risk analysis using distributions like the log-Pearson type III (LPIII) distribution, generalized extreme value (GEV) distribution, generalized Pareto distribution (GPD), and lognormal distribution, all of which assume stationarity of risk, is commonplace (Stedinger et al. 1993; Coles 2001; England et al. 2018). Several more recent approaches assess time-varying (i.e., nonstationary) characteristics of flood risk. AghaKouchak et al. (2013) and Salas et al. (2018) provide a detailed review of nonstationary extreme value analysis methods. Applying a nonstationary GEV distribution and allowing the location and/or scale of the distribution to change linearly as a function of time or various hydrometeorological covariates is one approach to assess changing flood risk (Coles 2001; Salas and Obeysekera 2014; Condon et al. 2015). This framework has been applied to extreme streamflow using time (Katz et al. 2002; Salas and Obeysekera 2014), meteorological variables (Towler et al. 2010; Condon et al. 2015), and climate indices (Lima et al. 2015) as covariates. Further, Condon et al. 2015 assessed future flood risk with this model framework using future projections of covariates generated from global climate models (GCMs).

For 12 National Park Service (NPS) sites (chosen to capture an array of hydroclimates in the U.S.) we project future 21st century flood risk by applying the nonstationary generalized extreme value distribution and projections of hydrometeorological variables from an ensemble of GCMs covering two Representative Concentration Pathways (RCP). There are few applications of nonstationary flood risk analysis to the management of U.S. public lands and conservation areas - the results presented in this work will help enable the NPS to better understand flood risks in a nonstationary context, which could subsequently be used for efficient short- and long-term management of protected resources.

2. Methods

Nonstationary Generalized Extreme Value Distribution

The starting point of the nonstationary flood frequency model is the assumption that the seasonal or annual flow extremes are assumed to follow the generalized extreme value distribution, a common statistical tool used in hydrological extreme value analysis. Described with further detail in Coles (2001), block maxima of independent and identically distributed random variables follow the generalized extreme value distribution, with the cumulative distribution function:

$$G(z) = exp\left\{-\left[1+\varepsilon\left(\frac{z-\mu}{\sigma}\right)\right]^{\frac{-1}{\varepsilon}}\right\} \tag{1}$$

where $\{z{:}1+\ \varepsilon(z-\mu)/\sigma\ \geq\ 0\}$. The variable z is the streamflow maxima and the parameters μ, σ, and ε represent the distribution location, scale, and shape, respectively. The location determines the position of the distribution, the scale determines the spread of the distribution, and the shape determines the behavior of the upper tail. Equation (1) follows the form of the type I extreme value distribution (EVI), or Gumbel distribution, when the shape (ε) is 0 (light tail). Similarly, equation (1) follows the form of the EVII, or Frechet distribution, when the shape (ε) is positive (heavy tail) and the EVIII, or Weibull distribution, when the shape is negative (bounded tail). Coles (2001) provides details on extreme value theory.

Nonstationarity is incorporated by allowing the location or both the location and scale parameters of equation (1) to vary as a function of covariates. The nonstationary location and scale are modeled as follows:

$$\mu(t) =\ \beta_{0,\mu} + \beta_{1,\mu}x_{1,\mathrm{t}} + \ldots + \beta_{n,\mu}x_{n,t} \tag{2}$$

$$\sigma(t) = exp\ (\ \beta_{0,\sigma} + \beta_{1,\sigma}x_{1,\mathrm{t}} + \ldots + \beta_{n,\sigma}x_{n,t}) \tag{3}$$

where x variables represent covariates and β denotes the fitted parameters. The transformed scale parameter is used to ensure the scale is positive. Stationary and nonstationary GEV parameters are estimated using the method of maximum likelihood (MLE), a general and flexible parameter estimation technique also used in similar studies (Katz et al. 2002; Towler et al. 2010; Condon et al. 2015).

The best nonstationary model (i.e. the best set of covariates) is selected by minimizing the Akaike Information Criteria (AIC), which penalizes the negative maximized log-likelihood of a model for the number of parameters used. AIC is defined by:

$$AIC =\ 2(NLLH) + 2(k) \tag{4}$$

where $NLLH$ is the negative maximized log-likelihood obtained from MLE and k is the number of independently adjusted model parameters (Akaike 1998). As an alternative to AIC, similar nonstationary GEV studies have used the likelihood ratio test, a common statistical tool used to test the significance of improvement in maximized log-likelihoods for nested models. However, with the number of models we test for in this study, outcomes of the likelihood ratio test would lose their interpretability (Katz 2013) and some of the models we fit are not nested. For this reason, the likelihood ratio test is not used as the primary selection criteria, though nonstationary models selected by AIC are still compared with the stationary GEV distribution with the likelihood ratio test.

Exceedance probability levels for stationary GEV distributions are solved with equation (5):

$$z_p = \mu - \frac{\sigma}{\varepsilon}\left[1 - \left\{-\ln\left(1-p\right)\right\}^{-\varepsilon}\right] \tag{5}$$

where z_p is the streamflow with exceedance probability p and the parameters μ, σ, and ε represent the GEV distribution location, scale, and shape (with $\varepsilon \neq 0$)(Coles 2001). Traditional stationary return level calculations are not applicable in a nonstationary context, where exceedance periods change with each new GEV distribution. We follow the methods explained in Salas and Obeysekera (2014) and Condon et al. (2015) for nonstationary risk assessment. The above methods were largely implemented in R (R Core Team 2016) with the package 'extRemes' (Gilleland and Katz 2016).

For comparison to the stationary and nonstationary GEV models, we also fit a stationary log-Pearson type III distribution to flow maxima. LPIII distributions are fit using the method of moments following USGS Bulletin #17B flood flow frequency guidelines (IACWD 1982). We include a visual process summary of stationary and nonstationary GEV flood frequency analysis in pages i-iii in Appendix A.

Here we assess future flood risk using an ensemble of climate model outputs (further described in subsequent sections). We first select a best nonstationary GEV distribution from a set of observed covariates. We then simulate model behavior with an ensemble of climate models to evaluate the risk of exceeding some site-specific critical flow within a selected design life. Steps for the analysis are:

1. A performance period of interest (e.g., 2040-2069), a project life (e.g., 20 years), and a critical flow are selected for a site.

2. One climate model is selected at random from the ensemble of climate models. From the randomly selected model, a block of covariate data is randomly selected within the period of interest and with a length of the project life (e.g., a 20-year block of data is selected from 2040-2069 model data).

3. The best nonstationary GEV distribution is applied to the selected block of covariate data to determine year-specific risks of exceeding the critical flow.

4. Following Salas and Obeysekera (2014), the total risk of exceeding the critical flow within the project life is calculated (e.g., the risk of exceeding the critical flow over the 20-year project life).

5. Steps 2-4 represent one simulation. This process is repeated for each RCP scenario, multiple climate models and the many blocks of covariate data with a length of the project life within the period of interest. This provides a distribution of simulated probabilities of exceeding the critical flow over the project life.

3. Study Sites and Data

Study Sites

Twelve USGS streamflow gauge sites of interest to the NPS are the focus of this study. Figure 1 provides details regarding the sites and their locations. These sites have a long historical USGS gauging record and represent a diverse array of hydroclimates where impactful flooding events occurred in the past. Further, these basins contain minimal hydrologic alteration, ensuring that human-caused land cover change and river alterations (e.g., diversions, dams, and other structures) are not impacting these study sites. Some recent notable and documented flood events for these basins include the January 1997 flood in Yosemite National Park, 2006 flooding in Mount Rainier National Park, and the 2017 flooding in the Ozark National Scenic Riverways.

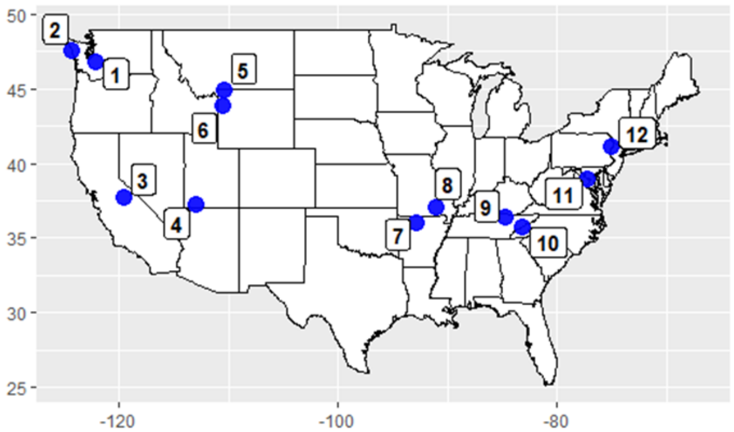

	USGS Site	USGS Site Description	Unit	Drainage Area (sq mi)
1	12082500	Nisqually River near National, WA	Mount Rainier National Park	133
2	12040500	Queets River near Clearwater, WA	Olympic National Park	445
3	11264500	Merced River at Happy Isles Bridge near Yosemite, CA	Yosemite National Park	181
4	09405500	North Fork Virgin River near Springdale, UT	Zion National Park	344
5	06188000	Lamar River near Tower Ranger Station, YNP	Yellowstone National Park	668
6	13011500	Pacific Creek at Moran, WY	Grand Teton National Park	169
7	07056000	Buffalo River near St. Joe, AR	Buffalo National River	829
8	07067000	Current River at Van Buren, MO	Ozark National Scenic Riverways	1,667
9	03409500	Clear Fork near Robbins, TN	Big South Fork National River and Recreation Area	272
10	03460000	Cataloochee Creek near Cataloochee, NC	Great Smoky Mountains National Park	49
11	01646500	Potomac River near Washington, D.C. Little Falls Pump	Chesapeake & Ohio Canal National Historical Park	11,560
12	01440000	Flat Brook near Flatbrookville, NJ	Delaware Water Gap National Recreation Area	64

Figure 1 Location (top) and descriptions (below) of the 12 sites.

Drainage areas of the selected basins range from 49 to 11,560 square miles. The sites have varied characteristics in terms of the timing of annual maxima, monthly precipitation, and streamflow seasonality, as shown in Figure 2. Sites in the northwest (Nisqually R. and Queets R.) experience flood events during the winter wet season. Western sites (Merced R., North Fork Virgin R., Lamar R., and Pacific Cr.) exhibit delayed spring streamflow response to winter precipitation, suggesting snowmelt driven river systems. Similarly, historical flooding events often occur in the spring for these sites, suggesting snowmelt might be an important driving mechanism for flooding events at these sites. The remaining eastern U.S. sites (Buffalo R., Current R., Clear Fork, Cataloochee Cr., Potomac R., and Flat Brook), exhibit variable streamflow and precipitation characteristics, with the majority of floods clustered over October-June.

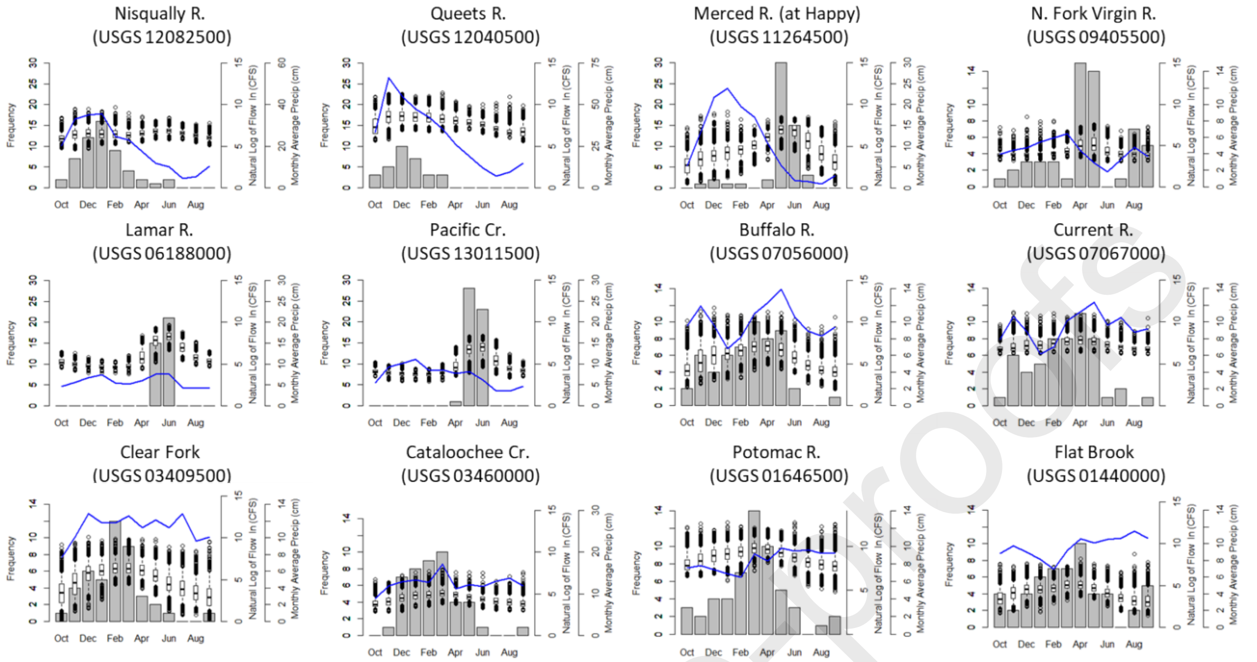

Figure 2 For each study site a bar plot for the count of annual peak mean daily flows occurring within each month (left axis), boxplots of mean daily flows for each month (right axis), and a line plot of average monthly precipitation (far right axis) using 1951-2005 data.

The months we use for seasonal analysis at each site are based on the timing of annual peak flows (water year), the distribution of daily flows for each month, and the monthly average precipitation. Generally, the season we select for analysis includes consecutive months that experience the highest frequency of annual maximum mean daily flows. We also assess monthly average precipitation and daily streamflow patterns to assess potential dominant flood mechanisms (e.g., runoff and snowmelt flood drivers), and we consider historical trends in the timing of observed seasonal peak flows. As further described in the coming section, the season we select to investigate for each site also corresponds to the seasonal covariates we use. To capture antecedent conditions that might influence flooding (e.g., snowpack), we also include covariates from the previous season.

Data

We use observed USGS gauge mean daily streamflow measurements available between 1951 and 2005 (water year) for analysis (U.S. Geological Survey 2016). Water years missing data within the season of interest are excluded from the analysis.

We use 1951-2005 (water year) observed season average daily precipitation of each contributing basin and season average daily hydrologic model generated flow as covariates – daily values of both are provided by the U.S. Bureau of Reclamation. These are determined using Livneh et al. (2015) 1/16^{o} spatially gridded meteorological data derived from NOAA Cooperative Observer Network stations. Hydrologic model flows provided by the U.S. Bureau of Reclamation are generated from the Variable Infiltration Capacity model (VIC). VIC is a land-surface model that simulates spatially gridded, land-atmosphere fluxes using the water and energy balance equations (Liang et al. 1994). Modeled flows are generated using VIC version 4.1.2h. This model requires daily precipitation, maximum and minimum air temperature, and wind speed as input forcings required (Prata 1996; Kimball et al. 1997; Thornton and Running 1999; Bohn et al. 2013). We use land-cover input data and calibrated parameters from Maurer et al. (2002) and Livneh et al. (2013). Details on the VIC model are available in: http://vic.readthedocs.io/en/master/. VIC river routing was performed at 1/16^o grids using the routing model from Lohmann et al. (1996).

The use of VIC model flows as a covariate in nonstationary flood frequency analysis is a novel contribution of this research. We introduce this because we posit that VIC model flows better capture the water and energy balance features of a basin as well as basin specific land-cover features compared to average meteorological covariates (e.g., precipitation). We assess and summarize VIC model performance compared to observed flows for each site and season in Table A-1; while the modeled flows for several of the sites have strong biases, the correlations between VIC model flows and observed streamflow for each site are strong. While the observed magnitude of daily flow (and potentially the observed magnitude of the seasonal peak daily flow) might be poorly captured by VIC model simulations, the seasonal average flow from the VIC model corresponded well with the observations and thus, is a valuable covariate. Furthermore, we found a strong correlation between seasonal average flows from the VIC model and the peak mean daily flow for the season of interest for each site (Table A-2). This suggests the seasonal average flows contain information about the seasonal peak flow; also, the VIC model flows capture the hydrologic processes in the basin providing complementary information. With this motivation, we use the seasonal average flows from VIC model as one of the covariates in the nonstationary GEV model.

We use an ensemble of projected 1951-2099 (water year) season average daily precipitation of each contributing basin and season average daily VIC model generated flow as future covariates, which enables 21st century projections of flood risk. Daily values of both are provided by the U.S. Bureau of Reclamation. Projections are determined using the U.S. Bureau of Reclamation’s LOCA CMIP5 dataset. This dataset contains 64 projections of daily, 1/16^o gridded precipitation and maximum/minimum temperature from an ensemble of 32 general circulation models, covering two different greenhouse gas RCPs. We investigate RCP 8.5, a scenario representing high and increasing greenhouse gas levels into the future, and RCP 4.5, a scenario representing a radiative forcing stabilization scenario (van Vuuren et al. 2011). LOCA CMIP5 data is generated from bias corrected and downscaled coarse GCM data (with a spatial resolution generally exceeding 1^o) from the CMIP5 multi-model ensemble (Taylor et al. 2011). Additional information on these processes can be found in Pierce et al. (2014, 2015) and Reclamation (2016). This data is available from the downscaled CMIP3 and CMIP5 climate and hydrology projections archive at https://gdo-dcp.ucllnl.org/downscaled_cmip_projections/. Information on the CMIP5 project can be found in Taylor et al. (2011). The GCMs we use through the LOCA CMIP5 dataset, the responsible modeling groups, and an acknowledgement of the World Climate Research Program's Working Group on Coupled Modelling are presented in Table A-3. The same methods as described earlier are used to generate VIC model flows. However, because average daily wind speed is not available in the LOCA CMIP5 dataset, historical Livneh et al. (2015) daily average wind speeds are used for the projected VIC wind speed forcing.

Overview

A process summary of this research appears in Figure 3. For each site of interest, we first fit a best nonstationary GEV model to observed historical seasonal peak flows considering historical season average and previous season average daily precipitation and hydrologic model generated flows as potential covariates. For each site a set of models is generated by fitting nonstationary GEV distributions to different combinations of these covariates, and, as mentioned, the best model (i.e., the best subset of covariates) is selected using AIC. We then apply to the best model for each site the LOCA CMIP5 ensemble of future covariate projections through 2099 (water year). For each year of each GCM ensemble member, the GEV distribution is projected using the projected covariate values. This provides time-varying estimates of flood frequency distributions into the future. We also include traditional flood frequency models (stationary GEV and LPIII distributions) in our analysis for comparison.

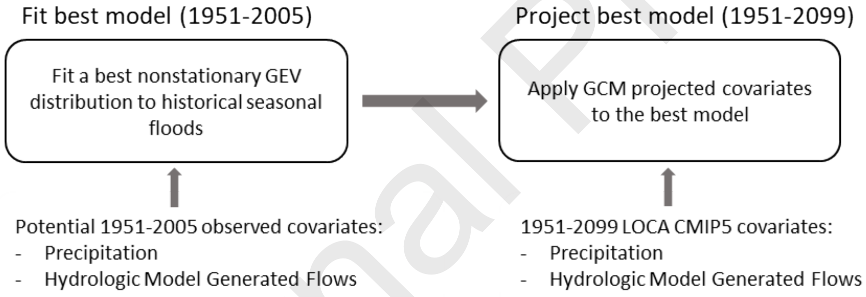

Figure 3 Process structure of this study.

4. Results

The best nonstationary GEV model was evaluated for each site using observed season and previous season average precipitation and VIC model flow as potential covariates. Table 1 lists the covariates selected in the best model for each park.

	USGS Site	USGS Site Description	Unit	Season of Analysis	Previous Season Covariates	GEV Location	GEV Scale	P-Value*
1	12082500	Nisqually River near National, WA	Mount Rainier National Park	Oct-Mar	Oct-Dec	VIC	VIC	3.8E-08
2	12040500	Queets River near Clearwater, WA	Olympic National Park	Oct-Mar	Oct-Dec	VIC		9.4E-05
3	11264500	Merced River at Happy Isles Bridge near Yosemite, CA	Yosemite National Park	Apr-Jun	Nov-Mar	Pre_Pr + Pr		<2.2E-16
4	09405500	North Fork Virgin River near Springdale, UT	Zion National Park	Apr-Jun	Nov-Mar	VIC	VIC	1.6E-13
5	06188000	Lamar River near Tower Ranger Station, YNP	Yellowstone National Park	Apr-Jun	Nov-Mar	Pre_VIC + VIC	Pre_VIC + VIC	8.8E-06
6	13011500	Pacific Creek at Moran, WY	Grand Teton National Park	Apr-Jun	Nov-Mar	Pre_Pr + Pr		4.2E-10
7	07056000	Buffalo River near St. Joe, AR	Buffalo National River	Jan-May	Oct-Dec	Pr	Pr	8.4E-10
8	07067000	Current River at Van Buren, MO	Ozark National Scenic Riverways	Feb-May	Nov-Jan	Pre_VIC + Pr	Pre_VIC + Pr	3.4E-11
9	03409500	Clear Fork near Robbins, TN	Big South Fork National River and Rec. Area	Dec-Mar	Oct-Nov	Pr		8.7E-07
10	03460000	Cataloochee Creek near Cataloochee, NC	Great Smoky Mountains National Park	Dec-Mar	Oct-Nov	VIC	VIC	2.0E-05
11	01646500	Potomac River near Washington, D.C. Little Falls Pump	Chesapeake & Ohio Canal National Hist. Park	Feb-May	Nov-Jan	VIC	VIC	8.7E-10
12	01440000	Flat Brook near Flatbrookville, NJ	Delaware Water Gap National Rec. Area	Feb-Apr	Nov-Jan	Pre_VIC + VIC	Pre_VIC + VIC	4.7E-09

Table 1 Best model parameters selected for the 12 sites. 'Pr' represents the seasonal average precipitation covariate and 'VIC' represents seasonal average flow covariate. A 'Pre' prefix indicates a previous season average covariate.

For all sites, nonstationary GEV distributions are selected over stationary GEV distributions based on AIC scores. The p-values from the likelihood ratio test (compared to the stationary GEV distribution) are also included, all of which are less than 0.05. VIC flows are selected as a covariate in the best model for eight of the sites while precipitation is selected in the best model for five of the sites. Five models select covariates from the previous season. The best models for eight of the sites have both a nonstationary location and scale. The remaining best models only have a nonstationary location, these are the sites with a blank in the 'GEV Scale' column of Table 1. Appendix B includes more detail on the site specific fitted parameter values for each best model. For all but two sites, the location and/or scale of the models shift upward with an increase in the selected covariate; higher previous season VIC flows for USGS 06188000 (Lamar River) and 01440000 (Flat Brook) result in a decrease in the GEV location and/or scale parameters. One possible explanation of this is that both of these sites experience winter snowfall, so a higher historical previous season VIC flow for these sites might suggest earlier winter snowmelt which will decrease the likelihood of obtaining high spring peak flows.

For each site, we use the best nonstationary GEV model (Table 1) and the ensemble of LOCA CMIP5 covariate projections to obtain an ensemble of 1% seasonal exceedance probability flows from 1951 to 2099 (water year). Because there are 64 model runs in the LOCA CMIP5 ensemble, 64 1% exceedance probability flows are generated for every year (32 for RCP 4.5 and 32 for RCP 8.5). 1% exceedance probability flows for each RCP scenario are grouped into approximately 30-year time periods from 1951 to 2099 (water year) and box plotted. The results for all sites appear in Figure 4. The 1% seasonal exceedance probability flows generated from the stationary LPIII distribution (blue line) and stationary GEV distribution (red line) fit to historical observed floods are also included. Similar plots for the 2% and 0.2% exceedance probability flows for each site are available in Appendix B.

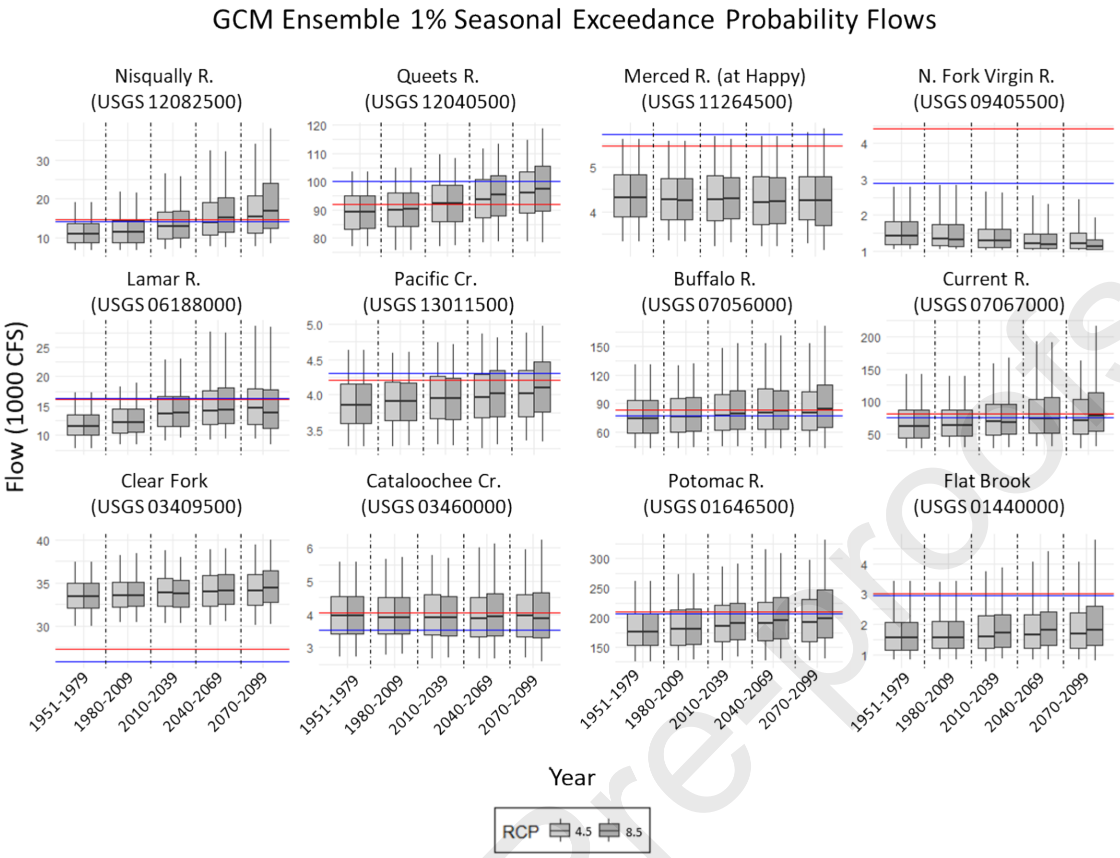

Figure 4 Boxplots of 1% exceedance probability flows generated from the best GEV model and LOCA CMIP5 covariate projections for each site. Stationary LPIII (blue line) and GEV (red line) 1% exceedance probability levels are also included.

For some sites (Nisqually R. and Queets R., for example), an increase in all quantiles of 1% exceedance probability flows generated from the LOCA CMIP5 ensemble into the future is apparent (shown as an upward shift in the boxplots over time). The opposite is apparent for USGS 09405500 (N. Fork Virgin R.), which is showing decreasing trends. For many of the sites (Buffalo R. and Current R., for example), we see an increase in the interquartile range and an increase in the difference between the 5th and 95th percentiles of the ensemble 1% exceedance probability flows. For a site like USGS 03460000 (Cataloochee River), where the median remains relatively steady, the changes in the interquartile range and 5th and 95th percentiles suggests an increase in variability in the magnitude of 1% exceedance probability flows generated by the LOCA CMIP5 ensemble. We see an increase in the difference between the 5th and 95th percentiles of the ensemble 1% exceedance probability flows for all but one site, which we address further in the discussion.

RCP 4.5 and RCP 8.5 ensemble trends are generally in agreement with one another for each site, with the RCP 8.5 ensemble typically having a stronger trend compared to the RCP 4.5 ensemble. When comparing the nonstationary 1% exceedance probability flows to those generated from the stationary LPIII and GEV distributions, for USGS 11264500 (Merced River), for example, from 1951-2099 generally between 75%-95% of the nonstationary 1% exceedance probability flows are below the stationary GEV 1% exceedance probability flow. This suggests that while the stationary GEV distribution might generally have a higher estimate of the seasonal 1% exceedance probability level, there are years where projected covariate conditions would indicate a higher seasonal 1% exceedance probability level with a nonstationary distribution. When calculating the risk of exceeding some threshold flow over a design life, if the design life includes a seasonal period where exceedance probability levels are large, the probability of exceeding that threshold flow will drastically increase. This will be captured in the simulation results explained further in the results section.

Results for USGS 03409500 (Clear Fork River) suggests stationary GEV and LPIII distributions estimate significantly lower 1% exceedance probability levels compared to the nonstationary model. Results specific to Clear Fork River in Appendix B show that nonstationary exceedance probability levels diverge from those of the stationary GEV model for larger exceedance probabilities. There are several extended periods of missing data for the Clear Fork River site, so limited data could be responsible for diverging performance between the stationary and nonstationary models for more extreme flows. The stationary and nonstationary GEV models generate very different 1% exceedance probability levels for USGS 09405500 (North Fork Virgin River). We found the stationary GEV distribution to poorly capture the more extreme observed historical floods. We also see from the likelihood ratio test there is a great degree of confidence (Table 1) that the log-likelihood of the nonstationary model is better than that of the stationary GEV distribution for this site.

A spatial plot of the percent change of the median 1% exceedance probability flow generated from the RCP 8.5 LOCA CMIP5 ensemble between the 1951-1979 and 2040-2069 periods for each site appears in Figure 5. We see a decrease in the median CMIP 1% seasonal exceedance flows for our study sites in the southwestern U.S. and an increase in the northern and eastern U.S.

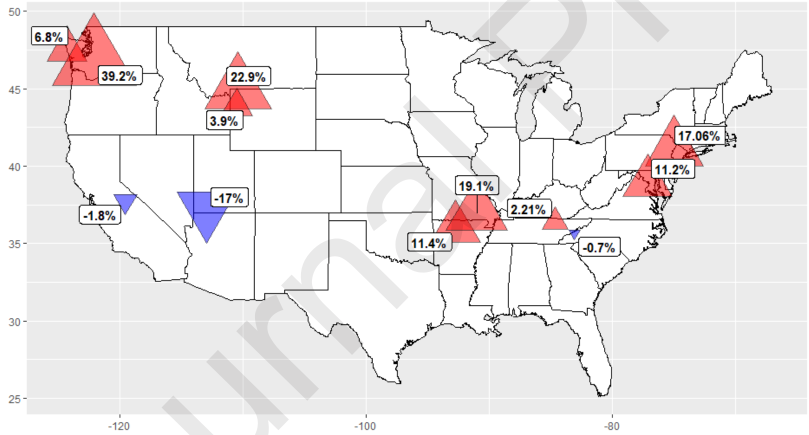

Figure 5 Percent change of RCP 8.5 2040-2069 median 1% seasonal exceedance flow compared to the 1951-1979 median 1% exceedance seasonal flow generated from the best GEV model and LOCA CMIP5 covariate projections for each site.

Using the best model and the LOCA CMIP5 ensemble at each site, we simulate the probability of exceeding a predetermined threshold flow over a specific design life. Here, we select a 20-year design life using the site's stationary GEV 1% exceedance probability flow as the threshold flow of interest. We run a large number of simulations for each site and boxplot simulation results. We separate simulations by the same 30-year periods and by RCP scenario as in Figure 4. Results are shared in Figure 6. Stationary GEV (red line) and LPIII (blue line) risks are also included. Similar plots for site specific critical flows are shared in Appendix B.

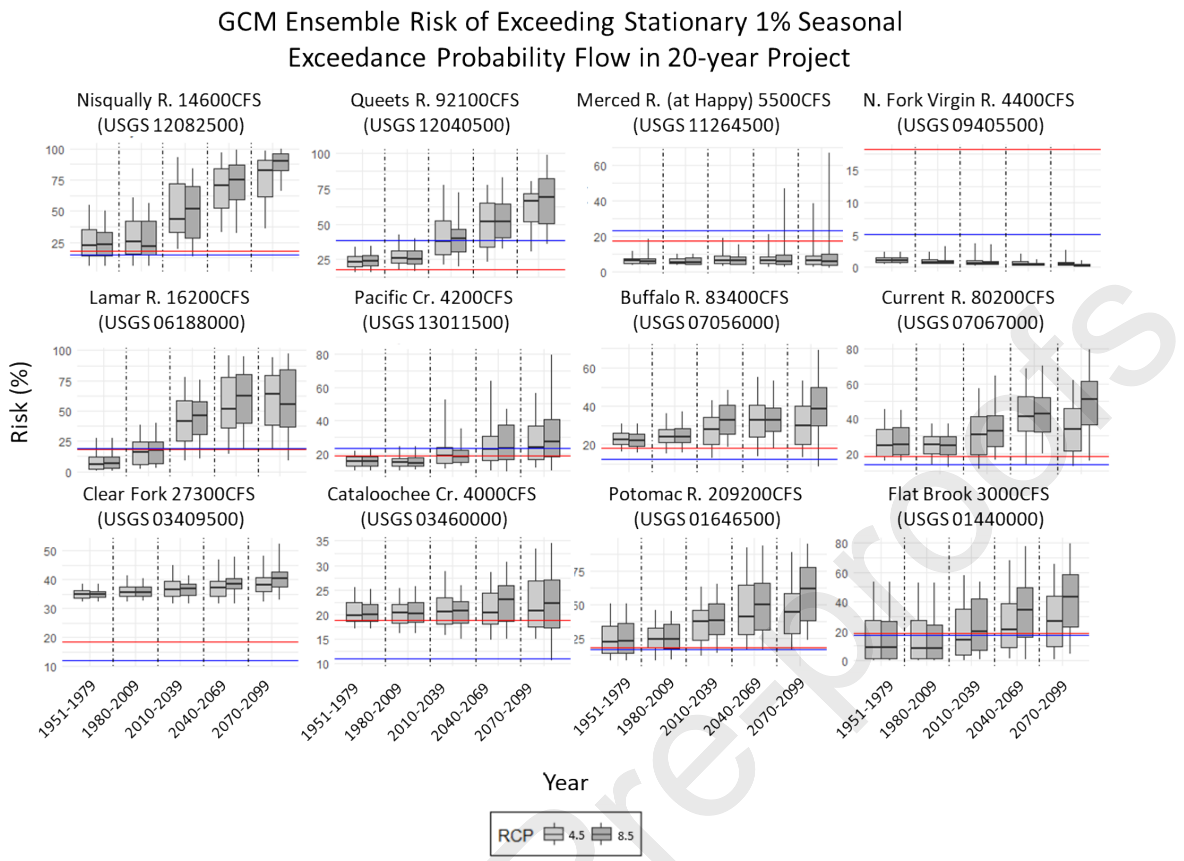

Figure 6 Simulation results for the risk of exceeding the site's stationary GEV 1% seasonal exceedance probability flow in a 20-year project life using the best nonstationary GEV model and LOCA CMIP5 covariate projections for each site (boxplots). Stationary LPIII (blue line) and GEV (red line) risks are also included.

While trends between Figure 4 and Figure 6 are similar, we generally see stronger trends in Figure 6. This is reasonable – a stronger trend will be present when a slight change in seasonal risk is compounded over 20 years. Further, as we saw in Figure 4, there are years within this LOCA CMIP5 ensemble where covariate conditions result in a much higher seasonal risk compared to the stationary distribution. If a high-risk season is included in a simulation's 20-year period, the risk of exceeding the threshold flow over the 20-year period will significantly increase.

5. Discussion and Conclusion

In this paper we utilize the nonstationary generalized extreme value distribution and an ensemble of climate models to project seasonal 21st century flood risk for twelve sites representing a diverse array of hydroclimates across the U.S. National Park Service. Results generally project a decrease in seasonal flood risk for sites in the southwestern U.S. and increases for sites in the eastern and northwestern U.S. These seasonal results display similar patterns to those identified by Hirsch and Ryberg (2012), who explored changes in historical flood magnitude under rising carbon dioxide levels at 200 sites across the U.S. Thus, our projections suggest the trends identified over the time period of Hirsch and Ryberg's work (where the median record length was 1916-2008) are likely to continue. Further, for many sites we find flows generated from a hydrologic model improved performance of nonstationary generalized extreme value distributions when used as covariates.

For long-term climate impact studies, two dominant sources of uncertainty arise when using an ensemble of climate models – future scenario uncertainty and model uncertainty (Hawkins and Sutton 2009). Described further in Deser et al. (2012), future scenario uncertainty can refer to, for example, uncertainty in greenhouse gas representative concentration pathway trajectories. Our results present only RCP 4.5 and RCP 8.5 scenarios, which typically display similar trends with stronger shifts in flood risk associated with RCP 8.5 trajectories. Model uncertainty arises from the fact that different climate models, given the same forcing, have different responses. As mentioned, for many of our sites, we see increases in the interquartile range and 5th-95th percentile range in our ensemble results presented in Figure 4 and Figure 6. This increase could relate to model uncertainty – climate models with different physical and numerical parameterizations can have diverging responses to long-term projections of input forcings. Our use of 32 GCMs, in part, characterizes this model uncertainty, and one common technique to combine results from climate ensembles involves taking a simple or weighted average of ensemble results (Tebaldi and Knutti 2007). The median and interquartile range in the boxplots presented in Figure 4 and Figure 6 represent this central tendency of the ensemble results, noting that we utilize the same 32 GCMs for each site and we do not assess individual GCM model performance for each site.

Our selection of covariates for the best model at each site assumes these general, seasonal average covariates represent the dominant driving mechanisms for seasonal peak flows; shifts in covariates suggest a shift in flood risk due to these dominant flood mechanisms. However, multiple flood generating mechanisms can be present (Berghuijs et al. 2016) and dominant flood mechanisms might exhibit long-term changes (e.g., transitions from snowmelt to rainfall-runoff) (Knowles et al. 2006; Das et al. 2013). For example, covariates like precipitation would not capture flood behavior shifts that arise from more precipitation falling as rainfall (as opposed to snowfall) in the future. This could be an advantage of using VIC model-generated flow as a covariate as we did here - shifting flood generating mechanism behavior for a basin can be better captured because VIC accounts for water and energy balance aspects of a system. In our study, VIC model generated flows are more frequently evident as a best model covariate over precipitation. Shifting dominant flood mechanisms might also shift the timing of peak floods out of the seasons studied in this paper, which cannot be accounted for in our covariates. Additionally, it is important to note the biases that remain in these VIC models (Table A-1) and in the LOCA CMIP5 dataset following bias correction and downscaling processes (Pierce et al. 2014, 2015).

We acknowledge this study does not assess nonstationary GEV model parameter uncertainties. Assessing standard errors from maximum likelihood estimates can provide more information on best model performance and exploring this method in a Bayesian framework could also be valuable for assessing uncertainties (Katz et al. 2002; Renard et al. 2013; Cheng et al. 2014; Bracken et al. 2018). Further, investigating the sensitivity of exceedance probability levels generated from the set of models we fit for each site (i.e., the models with different combinations of covariates) could also provide insight into model performance and the relationship between covariates and flood risk that these models capture.

Beyond investigating the uncertainties described above, future studies could investigate other flood characteristics like duration. Further, performing this analysis on each season of a year could provide more information on annual peak flood behavior for a particular site.

Overall our projected shifts in future flood behavior can help NPS managers assess the need to develop climate change informed flood risk management plans at different park units. This can improve risk mitigation for cultural and natural resources, inform site selection and design for roads, trails, and other infrastructure, and help managers proactively plan for trail and facility closures to ensure visitor safety. Due to the sensitive nature of flood planning for certain projects, we suggest utilizing these results, along with an in-depth understanding of specific basins and other industry accepted flood hazard evaluation techniques, to assess the factor of safety required for flood planning under a changing climate.

Acknowledgements

Funding for this research provided by the National Park Service under cooperative agreement P14AC00728 is gratefully acknowledged. We thank NPS managers who provided critical flow thresholds of interest to their parks. The manuscript was improved based on comments from two anonymous reviewers.

References

AghaKouchak A, Easterling D, Hsu K, et al (eds) (2013) Extremes in a Changing Climate, 1st edn. Springer, Netherlands, Dordrecht

Ahn K-H, Palmer RN (2016) Trend and Variability in Observed Hydrological Extremes in the United States. J Hydrol Eng 21:04015061. https://doi.org/10.1061/(ASCE)HE.1943-5584.0001286

Akaike H (1998) A New Look at the Statistical Model Identification. In: Parzen E, Tanabe K, Kitagawa G (eds) Selected Papers of Hirotugu Akaike. Springer New York, New York, NY, pp 215–222

Berghuijs WR, Woods RA, Hutton CJ, Sivapalan M (2016) Dominant flood generating mechanisms across the United States. Geophys Res Lett 43:4382–4390. https://doi.org/10.1002/2016GL068070

Bohn TJ, Livneh B, Oyler JW, et al (2013) Global evaluation of MTCLIM and related algorithms for forcing of ecological and hydrological models. Agric For Meteorol 176:38–49. https://doi.org/10.1016/j.agrformet.2013.03.003

Bracken C, Holman KD, Rajagopalan B, Moradkhani H (2018) A Bayesian Hierarchical Approach to Multivariate Nonstationary Hydrologic Frequency Analysis. Water Resour Res 54:243–255. https://doi.org/10.1002/2017WR020403

Cheng L, AghaKouchak A, Gilleland E, Katz RW (2014) Non-stationary extreme value analysis in a changing climate. Clim Change 127:353–369. https://doi.org/10.1007/s10584-014-1254-5

Coles S (2001) An introduction to statistical modeling of extreme values, 1st edn. Springer, London

Condon L, Gangopadhyay S, Pruitt T (2015) Climate change and non-stationary flood risk for the Upper Truckee River Basin. Hydrol Earth Syst Sci 19:159–175. https://doi.org/10.5194/hess-19-159-2015

Das T, Maurer EP, Pierce DW, et al (2013) Increases in flood magnitudes in California under warming climates. J Hydrol 501:101–110. https://doi.org/10.1016/j.jhydrol.2013.07.042

DeGaetano AT (2009) Time-Dependent Changes in Extreme-Precipitation Return-Period Amounts in the Continental United States. J Appl Meteorol Climatol 48:2086–2099. https://doi.org/10.1175/2009JAMC2179.1

Deser C, Phillips A, Bourdette V, Teng H (2012) Uncertainty in climate change projections: the role of internal variability. Clim Dyn 38:527–546. https://doi.org/10.1007/s00382-010-0977-x

England JF Jr, Cohn TA, Faber BA, et al (2018) Guidelines for determining flood flow frequency—Bulletin 17C: U.S. Geological Survey Techniques and Methods, book 4, chap. B5, 148 p.,. https://doi.org/https://doi.org/10.3133/tm4B5

Gilleland E, Katz RW (2016) {extRemes} 2.0: An Extreme Value Analysis Package in {R}. J Stat Softw 72:1--39. https://doi.org/10.18637/jss.v072.i08

Hartmann DL, Klein Tank AMG, Rusticucci M, et al (2013) Observations: Atmosphere and Surface. In: Stocker TF, Qin D, Plattner G-K, et al. (eds) Climate Change 2013: The Physical Science Basis.

Contribution of Working Group I to the Fifth Assessment Report of the Intergovernmental Panel on Climate Change. Cambridge University Press, Cambridge, United Kingdom and New York, NY, USA, pp 159–254

Hawkins E, Sutton R (2009) The Potential to Narrow Uncertainty in Regional Climate Predictions. Bull Am Meteorol Soc 90:1095–1108. https://doi.org/10.1175/2009BAMS2607.1

Hirsch RM, Ryberg KR (2012) Has the magnitude of floods across the USA changed with global CO2 levels? Hydrol Sci J 57:1–9. https://doi.org/10.1080/02626667.2011.621895

IACWD – Interagency Advisory Committee on Water Data (1982) Guidelines for determining flood flow frequency. Bulletin 17B of the Hydrology Subcommittee, Office of Water Data Coordination, US Geological Survey, Reston, VA

Katz RW (2013) Statistical Methods for Nonstationary Extremes. In: AghaKouchak A, Easterling D, Hsu K, et al. (eds) Extremes in a Changing Climate: Detection, Analysis and Uncertainty. Springer Netherlands, Dordrecht, pp 15–37

Katz RW, Parlange MB, Naveau P (2002) Statistics of extremes in hydrology. Adv Water Resour 25:1287–1304. https://doi.org/10.1016/S0309-1708(02)00056-8

Knowles N, Dettinger MD, Cayan DR (2006) Trends in Snowfall versus Rainfall in the Western United States. J Clim 19:4545–4559. https://doi.org/10.1175/JCLI3850.1

Liang X, Lettenmaier DP, Wood EF, Burges SJ (1994) A simple hydrologically based model of land surface water and energy fluxes for general circulation models. J Geophys Res 99:14415–14428. https://doi.org/10.1029/94JD00483

Lima CHR, Lall U, Troy TJ, Devineni N (2015) A climate informed model for nonstationary flood risk prediction: Application to Negro River at Manaus, Amazonia. J Hydrol 522:594–602. https://doi.org/10.1016/j.jhydrol.2015.01.009

Lins HF, Slack JR (1999) Streamflow trends in the United States. Geophys Res Lett 26:227–230. https://doi.org/10.1029/1998GL900291

Livneh B, Bohn TJ, Pierce DW, et al (2015) A spatially comprehensive, hydrometeorological data set for Mexico, the U.S., and Southern Canada 1950–2013. Sci Data 2:150042. https://doi.org/10.1038/sdata.2015.42

Livneh B, Rosenberg EA, Lin C, et al (2013) A Long-Term Hydrologically Based Dataset of Land Surface Fluxes and States for the Conterminous United States: Update and Extensions. J Clim 26:9384–9392. https://doi.org/10.1175/JCLI-D-12-00508.1

Lohmann D, Nolte-Holube R, Raschke E (1996) A large-scale horizontal routing model to be coupled to land surface parametrization schemes. Tellus A 48:708–721. https://doi.org/10.1034/j.1600-0870.1996.t01-3-00009.x

Mallakpour I, Villarini G (2015) The changing nature of flooding across the central United States. Nat Clim Change 5:250. https://doi.org/10.1038/nclimate2516

Milly PCD, Betancourt J, Falkenmark M, et al (2008) Stationarity Is Dead: Whither Water Management? Science 319:573. https://doi.org/10.1126/science.1151915

Pierce DW, Cayan DR, Maurer EP, et al (2015) Improved Bias Correction Techniques for Hydrological Simulations of Climate Change. J Hydrometeorol 16:2421–2442. https://doi.org/10.1175/JHM-D-14-0236.1

Pierce DW, Cayan DR, Thrasher BL (2014) Statistical Downscaling Using Localized Constructed Analogs (LOCA). J Hydrometeorol 15:2558–2585. https://doi.org/10.1175/JHM-D-14-0082.1

Prata AJ (1996) A new long-wave formula for estimating downward clear-sky radiation at the surface. Q J R Meteorol Soc 122:1127–1151. https://doi.org/10.1002/qj.49712253306

Reclamation (2016) Downscaled CMIP3 and CMIP5 Climate Projections - Addendum. Release of Downscaled CMIP5 Climate Projections (LOCA) and Comparison with Preceding Information. Prepared by the U.S. Department of the Interior, Bureau of Reclamation, Technical Services Center, Denver, Colorado. 29

Renard B, Sun X, Lang M (2013) Bayesian Methods for Non-stationary Extreme Value Analysis. In: AghaKouchak A, Easterling D, Hsu K, et al. (eds) Extremes in a Changing Climate: Detection, Analysis and Uncertainty. Springer Netherlands, Dordrecht, pp 39–95

Ross RJ, Elliott WP (1996) Tropospheric Water Vapor Climatology and Trends over North America: 1973–93. J Clim 9:3561–3574. https://doi.org/10.1175/1520-0442(1996)009<3561:TWVCAT>2.0.CO;2

Salas JD, Obeysekera J (2014) Revisiting the Concepts of Return Period and Risk for Nonstationary Hydrologic Extreme Events. J Hydrol Eng 19:554–568. https://doi.org/10.1061/(ASCE)HE.1943-5584.0000820

Salas JD, Obeysekera J, Vogel RM (2018) Techniques for assessing water infrastructure for nonstationary extreme events: a review. Hydrol Sci J 63:325–352. https://doi.org/10.1080/02626667.2018.1426858

Stedinger J, Vogel R, Foufoula-Georgiou E (1993) Frequency Analysis of Extreme Events. In: Maidment DR (ed) Handbook of Hydrology. McGraw Hill Book Company, New York

Taylor KE, Stouffer RJ, Meehl GA (2011) An Overview of CMIP5 and the Experiment Design. Bull Am Meteorol Soc 93:485–498. https://doi.org/10.1175/BAMS-D-11-00094.1

Tebaldi C, Knutti R (2007) The use of the multi-model ensemble in probabilistic climate projections. Philos Trans R Soc Math Phys Eng Sci 365:2053–2075. https://doi.org/10.1098/rsta.2007.2076

Thornton PE, Running SW (1999) An improved algorithm for estimating incident daily solar radiation from measurements of temperature, humidity, and precipitation. Agric For Meteorol 93:211–228. https://doi.org/10.1016/S0168-1923(98)00126-9

Towler E, Rajagopalan B, Gilleland E, et al (2010) Modeling hydrologic and water quality extremes in a changing climate: A statistical approach based on extreme value theory. Water Resour Res 46:. https://doi.org/10.1029/2009WR008876

Trenberth KE, Dai A, Rasmussen RM, Parsons DB (2003) The Changing Character of Precipitation. Bull Am Meteorol Soc 84:1205–1218. https://doi.org/10.1175/BAMS-84-9-1205

U.S. Geological Survey (2016) U.S. Geological Survey, 2016, National Water Information System data available on the World Wide Web (USGS Water Data for the Nation), accessed [April 15, 2018], at URL [http://waterdata.usgs.gov/nwis/].

van Vuuren DP, Edmonds J, Kainuma M, et al (2011) The representative concentration pathways: an overview. Clim Change 109:5. https://doi.org/10.1007/s10584-011-0148-z

Wasko C, Sharma A (2017) Global assessment of flood and storm extremes with increased temperatures. Scientific Reports 7:7945. https://doi.org/10.1038/s41598-017-08481-1

Appendix A

The following pages i-iii include a process summary of the stationary and nonstationary flood frequency analysis used in this paper. The process in these pages is demonstrated in an ***annual*** *timeframe, though it is just as applicable to a* ***seasonal*** *timeframe.*

Stationary Flood Risk

1. Select Annual Maxima

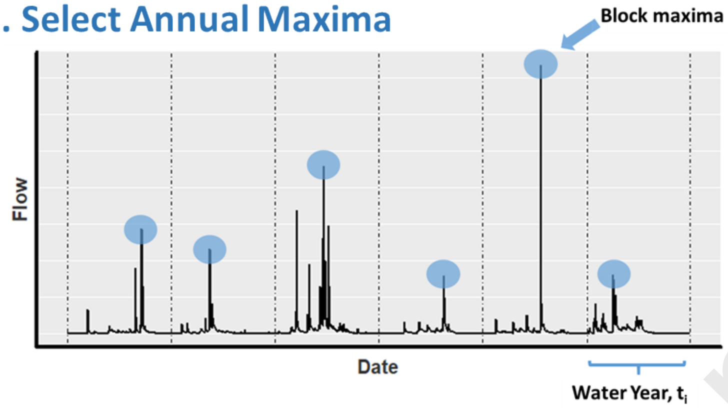

The set of annual maximum flows (i.e., the block maxima) is determined

2. Fit a GEV Distribution to Block Maxima

A stationary generalized extreme value (GEV) distribution is fit to the bock maxima

$$\mathrm{F}(x) = \boldsymbol{exp}\left\{-\left[\mathbf{1}+\boldsymbol{\varepsilon}\frac{(\mathbf{x}-\boldsymbol{\mu})}{\boldsymbol{\sigma}}\right]^{\frac{-\mathbf{1}}{\boldsymbol{\varepsilon}}}\right\}$$

The stationary GEV distribution is defined by 3 parameters:

location (μ), scale (σ), and shape (ε)

We estimate these parameters using the method of maximum likelihood

μ	ϕ	ε
1406.0	994.3	0.6

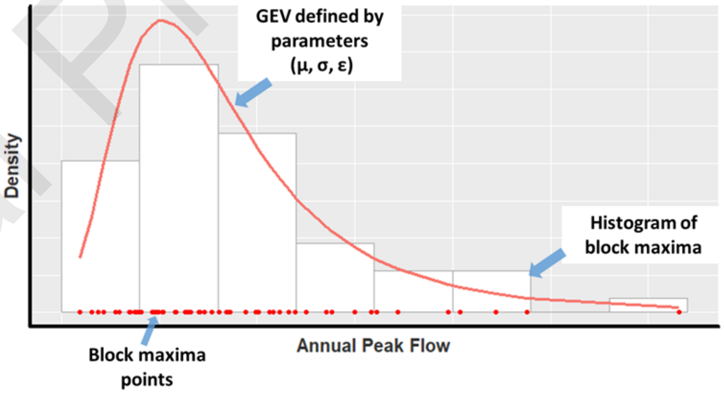

3. Calculate Risk of Flood

The fit distribution is used to assess the risk of exceeding a flow

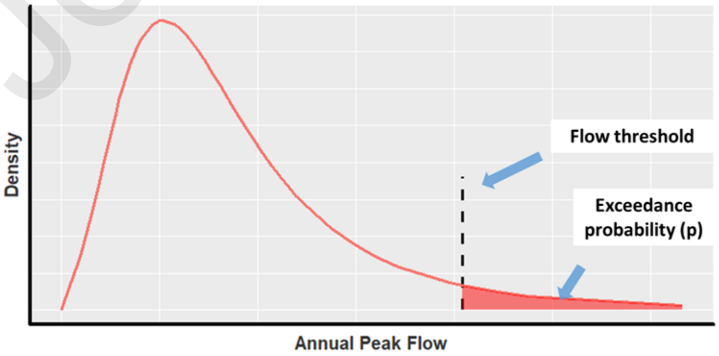

$$\mathbf{R} = \mathbf{1} - (\mathbf{1} - \boldsymbol{p})^{\boldsymbol{n}}$$

Risk of flood occurring in n years

Probability of flow above flood threshold occurring in any year

Non-Stationary Flood Risk

1. Select Annual Maxima

The set of annual maximum flows (i.e., the block maxima) is determined

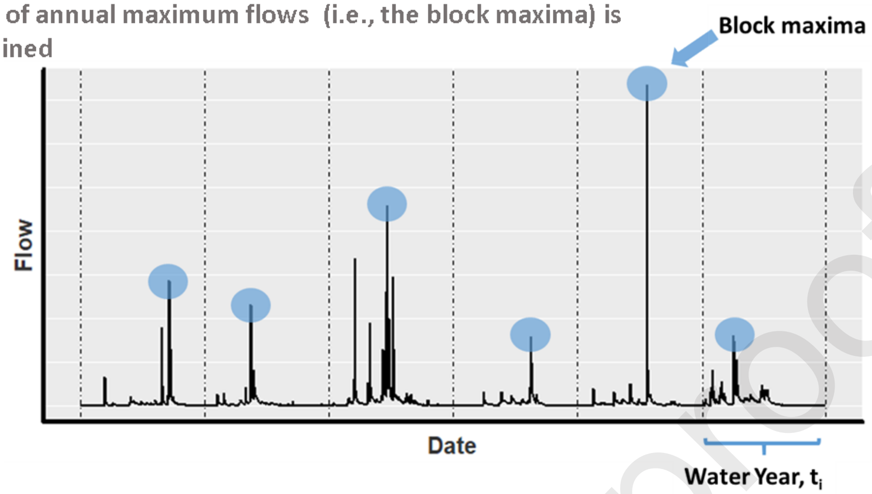

2. Fit a Non-Stationary GEV Distribution to Block Maxima

A non-stationary generalized extreme value (GEV) distribution is fit to the bock maxima.

A non-stationary GEV distribution allows the location (μ) and scale (σ) parameters to vary with meteorological variables. In this case, the location and scale vary with annual precipitation. However, other climate covariates are often used.

$$\mathrm{F}(x) = exp\left\{-\left[1+\varepsilon\frac{(\mathrm{x}-\mu(t))}{\sigma(t)}\right]^{\frac{-1}{\varepsilon}}\right\}$$

$$\mu(t) = \beta_0 + \beta_1 Pr_t$$
$$\sigma(t) = \alpha_0 + \alpha_1 Pr_t$$
$$\varepsilon = \text{constant}$$

The location and scale shift as a function of precipitation. This GEV distribution is defined by 5 parameters ($\beta_0, \beta_1, \alpha_0, \alpha_1$, ε)

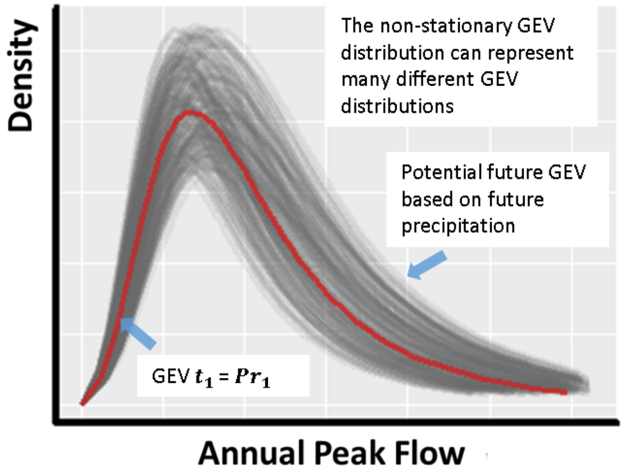

The non-stationary GEV distribution can represent many different GEV distributions

Potential future GEV based on future precipitation

β_0	β_1	α_0	α_1	ε	Nllh	AIC
1324.2	115.8	6.8	0.1	0.2	463.2	936.5

LR Test Against Stationary GEV Model: **p-value=0.02**

We solve for the 5 parameters using the method of maximum likelihood and assess the model fit using AIC and a likelihood ratio test.

3. Determine the GEV Distribution for Every Time Period

Using the annual precipitation covariate and the fit non-stationary GEV model, a location and scale is determined for each year

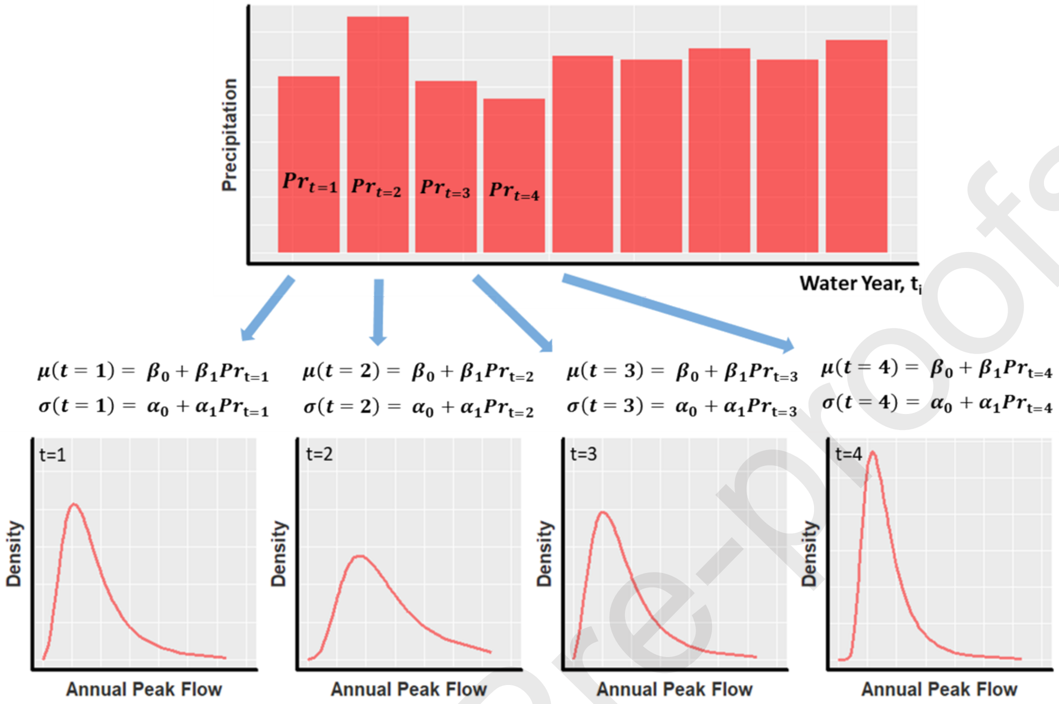

4. Calculate Risk by Combining GEVs Calculated for Each Step

The fit distribution is used to assess the risk of exceeding a flow. Because the non-stationary GEV model defines a different location and scale for each year (depending on annual precipitation), the risk of exceeding a flow changes between years.

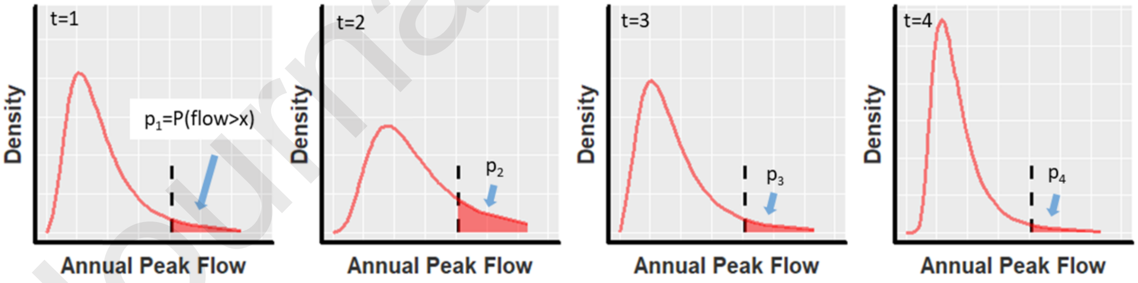

$$\mathbf{R} = \mathbf{1} - \prod_{t=1}^{n} (\mathbf{1} - \boldsymbol{p_t})$$

In this case, the risk calculated is specific to years t=1 to t=4. Different GEVs, and therefore a different risk, will occur in years t=5 to t=8, for example.

				VIC Model Skill Scores		
	USGS Site	**USGS Site Description**	**Season**	**NSE**	**COR**	**PBIAS (%)**
1	12082500	Nisqually River near National, WA	Oct-Mar	-0.19	0.67	-42.0
			Oct-Dec	-0.05	0.79	-45.9
2	12040500	Queets River near Clearwater, WA	Oct-Mar	0.62	0.92	-23.9
			Oct-Dec	0.65	0.93	-27.7
3	11264500	Merced River at Happy Isles Bridge near Yosemite, CA	Apr-Jun	-0.42	0.78	19.3
			Nov-Mar	-0.05	0.69	-72.1
4	09405500	North Fork Virgin River near Springdale, UT	Apr-Jun	0.34	0.79	-1.7
			Nov-Mar	-1.30	0.66	-11.8
5	06188000	Lamar River near Tower Ranger Station, YNP	Apr-Jun	-0.46	0.77	-69.4
			Nov-Mar	-1.20	0.53	-4.1
6	13011500	Pacific Creek at Moran, WY	Apr-Jun	0.26	0.82	-48.6
			Nov-Mar	-0.16	0.61	-19.4
7	07056000	Buffalo River near St. Joe, AR	Jan-May	0.77	0.89	-14.1
			Oct-Dec	0.87	0.95	21.2
8	07067000	Current River at Van Buren, MO	Feb-May	0.55	0.82	-9.8
			Nov-Jan	0.55	0.92	20.6
9	03409500	Clear Fork near Robbins, TN	Dec-Mar	0.53	0.82	-23.4
			Oct-Nov	0.37	0.85	-28.5
10	03460000	Cataloochee Creek near Cataloochee, NC	Dec-Mar	0.18	0.87	19.8
			Oct-Nov	0.60	0.93	-6.0
11	01646500	Potomac River near Washington, D.C. Little Falls Pump	Feb-May	0.71	0.85	-6.0
			Nov-Jan	0.59	0.84	27.3
12	01440000	Flat Brook near Flatbrookville, NJ	Feb-Apr	0.43	0.78	-20.6
			Nov-Jan	0.64	0.82	-10.2

Table A-1 Monthly VIC model flow performance metrics over seasons of interest (using observed historical forcings from 1951-2005 water years) for each study site. Metrics include the Nash-Sutcliffe efficiency, Pearson correlation, and percent bias.

	USGS Site	**USGS Site Description**	**Season**	**COR**
1	12082500	Nisqually River near National, WA	Oct-Mar	0.68
			Oct-Dec	0.59
2	12040500	Queets River near Clearwater, WA	Oct-Mar	0.62
			Oct-Dec	0.50
3	11264500	Merced River at Happy Isles Bridge near Yosemite, CA	Apr-Jun	0.72
			Nov-Mar	0.14
4	09405500	North Fork Virgin River near Springdale, UT	Apr-Jun	0.80
			Nov-Mar	0.55
5	06188000	Lamar River near Tower Ranger Station, YNP	Apr-Jun	0.52
			Nov-Mar	-0.09
6	13011500	Pacific Creek at Moran, WY	Apr-Jun	0.69
			Nov-Mar	0.12
7	07056000	Buffalo River near St. Joe, AR	Jan-May	0.61
			Oct-Dec	-0.05
8	07067000	Current River at Van Buren, MO	Feb-May	0.60
			Nov-Jan	0.26
9	03409500	Clear Fork near Robbins, TN	Dec-Mar	0.59
			Oct-Nov	-0.03
10	03460000	Cataloochee Creek near Cataloochee, NC	Dec-Mar	0.50
			Oct-Nov	0.32
11	01646500	Potomac River near Washington, D.C. Little Falls Pump	Feb-May	0.70
			Nov-Jan	0.30
12	01440000	Flat Brook near Flatbrookville, NJ	Feb-Apr	0.65
			Nov-Jan	0.03

Table A-2 Correlations between season of interest and previous season of interest average mean daily VIC model flow and the site's season of interest peak mean daily flow. For each site, the top set of months correspond to the season of interest and the bottom set of months corresponding to the previous season of interest.

Modeling Center (or Group)	Institute ID	Model Name
Commonwealth Scientific and Industrial Research Organization (CSIRO) and Bureau of Meteorology (BOM), Australia	CSIRO-BOM	ACCESS1.0 ACCESS1.3
Beijing Climate Center, China Meteorological Administration	BCC	BCC-CSM1.1 BCC-CSM1.1(m)
Canadian Centre for Climate Modelling and Analysis	CCCMA	CanESM2
National Center for Atmospheric Research	NCAR	CCSM4
Community Earth System Model Contributors	NSF-DOE-NCAR	CESM1(BGC) CESM1(CAM5)
Centro Euro-Mediterraneo per I Cambiamenti Climatici	CMCC	CMCC-CM CMCC-CMS
Centre National de Recherches Météorologiques / Centre Européen de Recherche et Formation Avancée en Calcul Scientifique	CNRM-CERFACS	CNRM-CM5
Commonwealth Scientific and Industrial Research Organization in collaboration with Queensland Climate Change Centre of Excellence	CSIRO-QCCCE	CSIRO-Mk3.6.0
EC-EARTH consortium	EC-EARTH	EC-EARTH
LASG, Institute of Atmospheric Physics, Chinese Academy of Sciences and CESS, Tsinghua University	LASG-CESS	FGOALS-g2
NOAA Geophysical Fluid Dynamics Laboratory	NOAA GFDL	GFDL-CM3 GFDL-ESM2G GFDL-ESM2M
NASA Goddard Institute for Space Studies	NASA GISS	GISS-E2-H GISS-E2-R
National Institute of Meteorological Research/Korea Meteorological Administration	NIMR/KMA	HadGEM2-AO
Met Office Hadley Centre (additional HadGEM2-ES realizations contributed by Instituto Nacional de Pesquisas Espaciais)	MOHC (additional realizations by INPE)	HadGEM2-CC HadGEM2-ES
Institute for Numerical Mathematics	INM	INM-CM4
Institut Pierre-Simon Laplace	IPSL	IPSL-CM5A-LR IPSL-CM5A-MR
Japan Agency for Marine-Earth Science and Technology, Atmosphere and Ocean Research Institute (The University of Tokyo), and National Institute for Environmental Studies	MIROC	MIROC-ESM MIROC-ESM-CHEM
Atmosphere and Ocean Research Institute (The University of Tokyo), National Institute for Environmental Studies, and Japan Agency for Marine-Earth Science and Technology	MIROC	MIROC5
Max-Planck-Institut für Meteorologie (Max Planck Institute for Meteorology)	MPI-M	MPI-ESM-MR MPI-ESM-LR
Meteorological Research Institute	MRI	MRI-CGCM3
Norwegian Climate Centre	NCC	NorESM1-M

Table A-3 The 32 CMIP5 models in the LOCA CMIP5 ensemble. We acknowledge the World Climate Research Program's Working Group on Coupled Modelling, which is responsible for CMIP, and we thank the climate modeling groups for producing and making available their model output. For CMIP the U.S. Department of Energy's Program for Climate Model Diagnosis and Intercomparison provides coordinating support and led development of software infrastructure in partnership with the Global Organization for Earth System Science Portals.

Appendix B

Seasonal Flow Analysis

The following pages contain seasonal flood frequency results for all 12 sites. Sites and the season of interest are shared in the table below.

	USGS Site	USGS Site Description	Unit	Season of Analysis	Previous Season Covariates
1	12082500	Nisqually River near National, WA	Mount Rainier National Park	Oct-Mar	Oct-Dec
2	12040500	Queets River near Clearwater, WA	Olympic National Park	Oct-Mar	Oct-Dec
3	11264500	Merced River at Happy Isles Bridge near Yosemite, CA	Yosemite National Park	Apr-Jun	Nov-Mar
4	09405500	North Fork Virgin River near Springdale, UT	Zion National Park	Apr-Jun	Nov-Mar
5	06188000	Lamar River near Tower Ranger Station, YNP	Yellowstone National Park	Apr-Jun	Nov-Mar
6	13011500	Pacific Creek at Moran, WY	Grand Teton National Park	Apr-Jun	Nov-Mar
7	07056000	Buffalo River near St. Joe, AR	Buffalo National River	Jan-May	Oct-Dec
8	07067000	Current River at Van Buren, MO	Ozark National Scenic Riverways	Feb-May	Nov-Jan
9	03409500	Clear Fork near Robbins, TN	Big South Fork National River and Rec. Area	Dec-Mar	Oct-Nov
10	03460000	Cataloochee Creek near Cataloochee, NC	Great Smoky Mountains National Park	Dec-Mar	Oct-Nov
11	01646500	Potomac River near Washington, D.C. Little Falls Pump	Chesapeake & Ohio Canal National Hist. Park	Feb-May	Nov-Jan
12	01440000	Flat Brook near Flatbrookville, NJ	Delaware Water Gap National Rec. Area	Feb-Apr	Nov-Jan

Seasonal Extreme Flow Analysis

Nisqually River near National, WA (USGS 12082500)
Mount Rainier National Park

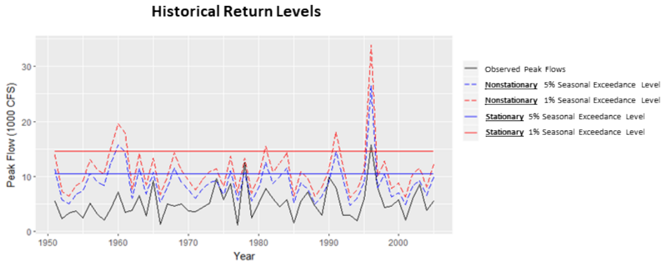

Figure 1 (above): A comparison of historical 5% and 1% stationary GEV and best nonstationary GEV return levels. Gaps represent missing data.

Best Nonstationary GEV Model

Location ~ VIC, Scale ~ VIC							
Location		**Scale**					
μ_0	μ_1	ϕ_0	ϕ_1	**Shape**	**Nllh**	**AIC**	**BIC**
-0.35	10.33	-0.46	1.998	-0.05	109.7	229.5	239.5
LR Test Against Stationary GEV Model: **p-value=3.842e-08**							

Table 1: Fitted parameter values and skill scores for the best nonstationary GEV model.

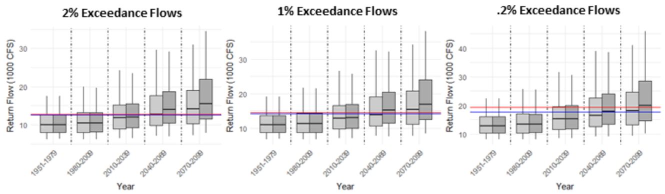

Figure 2 (above): Stationary GEV and LPIII return levels (solid lines) and boxplots of nonstationary return levels generated from the LOCA CMIP5 ensemble of covariates. Results cover two RCP scenarios.

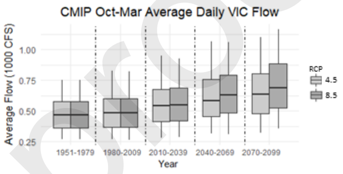

Figure 3 (above): Boxplots of LOCA CMIP5 ensemble covariates. Results cover two RCP scenarios.

Return Flow (1000 CFS)

Exceedance Probability	**Stationary Models**		**Nonstationary GEV Model - GCM Ensemble Percentile**									
	GEV	**LPIII**	**RCP**	**1980-2009**			**2040-2069**			**2070-2099**		
				25th	Median	75th	25th	Median	75th	25th	Median	75th
20%	7.0	7.2	4.5	5.3	7.0	8.9	6.6	8.6	11.6	6.9	9.5	12.5
			8.5	5.4	7.0	8.9	7.1	9.4	12.3	7.7	10.3	14.2
10%	8.7	8.9	4.5	6.2	8.1	10.3	7.6	10.0	13.6	8.0	11.0	14.7
			8.5	6.3	8.2	10.3	8.2	10.9	14.4	8.9	12.0	16.7
4%	11.0	11.0	4.5	7.3	9.5	12.0	8.9	11.6	15.9	9.4	12.8	17.2
			8.5	7.3	9.5	12.0	9.5	12.7	16.9	10.4	14.1	19.7
1%	14.6	14.2	4.5	8.8	11.4	14.4	10.7	13.9	19.2	11.2	15.4	20.8
			8.5	8.8	11.4	14.4	11.4	15.2	20.4	12.5	16.9	23.9

Table 2 (above): Stationary GEV and LPIII return levels and best nonstationary GEV return levels. Percentiles for nonstationary return levels represent the percentile return level from the LOCA CMIP5 ensemble within the specified time period. Results cover two RCP scenarios.

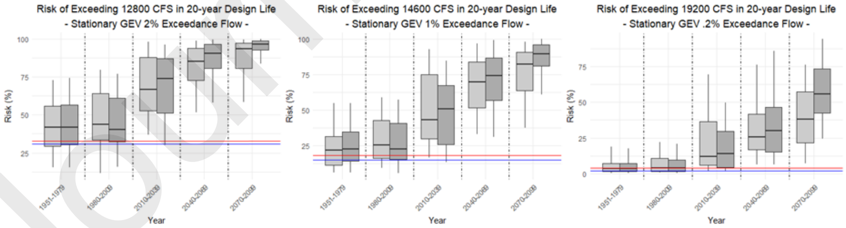

Figure 4 (left): Risk of exceeding critical flows within design life for stationary GEV and LPIII models (solid lines) and best nonstationary GEV model simulations from the LOCA CMIP5 ensemble of covariates (boxplots).

Seasonal Extreme Flow Analysis

Queets River near Clearwater, WA (USGS 12040500)
Olympic National Park

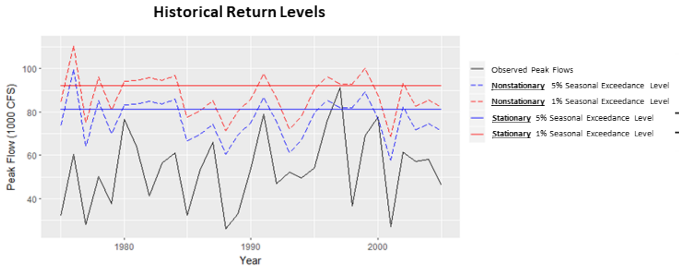

Figure 1 (above): A comparison of historical 5% and 1% stationary GEV and best nonstationary GEV return levels. Gaps represent missing data.

Best Nonstationary GEV Model

Location ~ VIC

Location						
μ_0	**μ_1**	**Scale**	**Shape**	**Nllh**	**AIC**	**BIC**
11.85	7.04	11.95	-0.15	123.3	254.5	260.3

LR Test Against Stationary GEV Model: **p-value=9.403e-05**

Table 1: Fitted parameter values and skill scores for the best nonstationary GEV model.

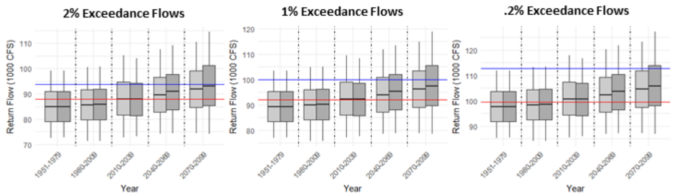

Figure 2 (above): Stationary GEV and LPIII return levels (solid lines) and boxplots of nonstationary return levels generated from the LOCA CMIP5 ensemble of covariates. Results cover two RCP scenarios.

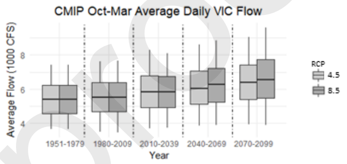

Figure 3 (above): Boxplots of LOCA CMIP5 ensemble covariates. Results cover two RCP scenarios.

Return Flow (1000 CFS)

	Stationary Models		Nonstationary GEV Model - GCM Ensemble Percentile									
Exceedance Probability	**GEV**	**LPIII**	**RCP**		**1980-2009**			**2040-2069**			**2070-2099**	
				25th	Median	75th	25th	Median	75th	25th	Median	75th
20%	67.4	67.7	4.5	60.7	66.6	72.7	63.8	70.4	77.6	65.7	72.7	80.0
			8.5	60.8	66.8	72.7	64.6	71.9	78.7	66.4	74.0	82.2
10%	75.1	76.8	4.5	67.5	73.4	79.4	70.5	77.1	84.3	72.5	79.5	86.8
			8.5	67.5	73.5	79.4	71.4	78.6	85.4	73.1	80.7	88.9
4%	83.1	87.0	4.5	74.9	80.8	86.9	77.9	84.6	91.8	79.9	86.9	94.2
			8.5	74.9	81.0	86.9	78.8	86.1	92.9	80.6	88.2	96.4
1%	92.1	100.0	4.5	84.1	90.0	96.1	87.1	93.8	101.0	89.1	96.1	103.4
			8.5	84.1	90.2	96.1	88.0	95.3	102.1	89.8	97.4	105.6

Table 2 (above): Stationary GEV and LPIII return levels and best nonstationary GEV return levels. Percentiles for nonstationary return levels represent the percentile return level from the LOCA CMIP5 ensemble within the specified time period. Results cover two RCP scenarios.

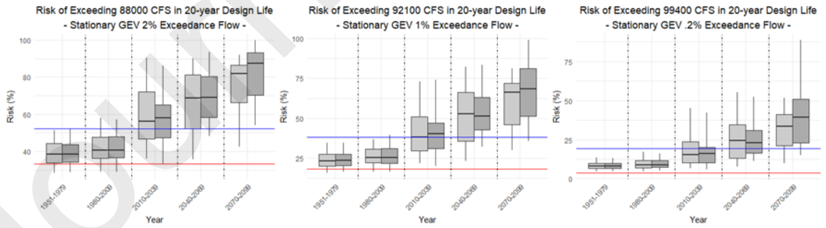

Figure 4 (left): Risk of exceeding critical flows within design life for stationary GEV and LPIII models (solid lines) and best nonstationary GEV model simulations from the LOCA CMIP5 ensemble of covariates (boxplots).

Seasonal Extreme Flow Analysis

Merced River at Happy Isles Bridge near Yosemite, CA (USGS 11264500)
Yosemite National Park

Historical Return Levels

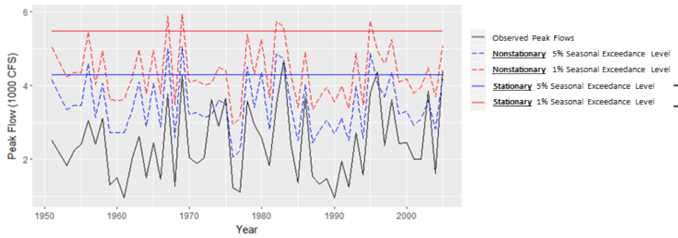

Figure 1 (above): A comparison of historical 5% and 1% stationary GEV and best nonstationary GEV return levels. Gaps represent missing data.

Best Nonstationary GEV Model

Location ~ Pre_Pr + Pr

Location							
μ_0	μ_1	μ_2	**Scale**	**Shape**	**Nllh**	**AIC**	**BIC**
0.11	0.24	0.29	0.37	0.10	35.0	79.9	89.9

LR Test Against Stationary GEV Model: **p-value < 2.2e-16**

Table 1: Fitted parameter values and skill scores for the best nonstationary GEV model.

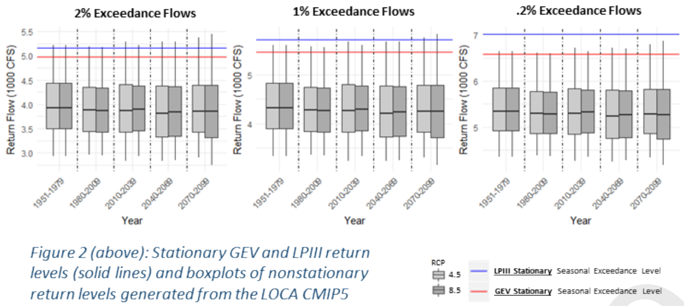

Figure 2 (above): Stationary GEV and LPIII return levels (solid lines) and boxplots of nonstationary return levels generated from the LOCA CMIP5 ensemble of covariates. Results cover two RCP scenarios.

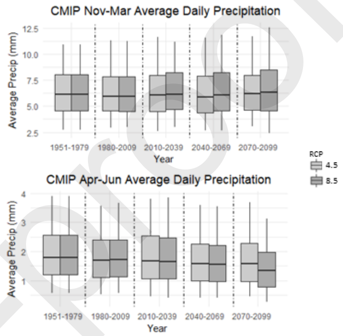

Figure 3 (above): Boxplots of LOCA CMIP5 ensemble covariates. Results cover two RCP scenarios.

Return Flow (1000 CFS)

	Stationary Models		**Nonstationary GEV Model - GCM Ensemble Percentile**									
Exceedance Probability	**GEV**	**LPIII**	**RCP**	**1980-2009**			**2040-2069**			**2070-2099**		
				25th	Median	75th	25th	Median	75th	25th	Median	75th
20%	3.2	3.2	4.5	2.3	2.7	3.2	2.2	2.6	3.2	2.3	2.7	3.2
			8.5	2.3	2.7	3.2	2.2	2.7	3.2	2.2	2.7	3.2
10%	3.8	3.8	4.5	2.6	3.0	3.5	2.5	3.0	3.6	2.6	3.0	3.6
			8.5	2.6	3.0	3.5	2.5	3.0	3.5	2.5	3.0	3.6
4%	4.5	4.6	4.5	3.1	3.5	4.0	3.0	3.4	4.0	3.1	3.5	4.0
			8.5	3.1	3.5	4.0	3.0	3.5	4.0	2.9	3.5	4.0
1%	5.5	5.7	4.5	3.8	4.3	4.7	3.7	4.2	4.8	3.8	4.2	4.8
			8.5	3.8	4.3	4.7	3.7	4.2	4.8	3.7	4.2	4.8

Table 2 (above): Stationary GEV and LPIII return levels and best nonstationary GEV return levels. Percentiles for nonstationary return levels represent the percentile return level from the LOCA CMIP5 ensemble within the specified time period. Results cover two RCP scenarios.

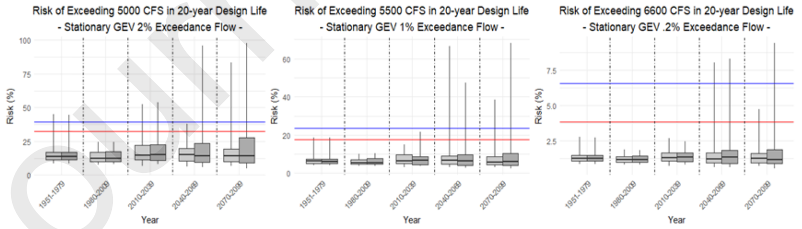

Figure 4 (left): Risk of exceeding critical flows within design life for stationary GEV and LPIII models (solid lines) and best nonstationary GEV model simulations from the LOCA CMIP5 ensemble of covariates (boxplots).

Seasonal Extreme Flow Analysis

North Fork Virgin River near Springdale, UT (USGS 09405500)
Zion National Park

Historical Return Levels

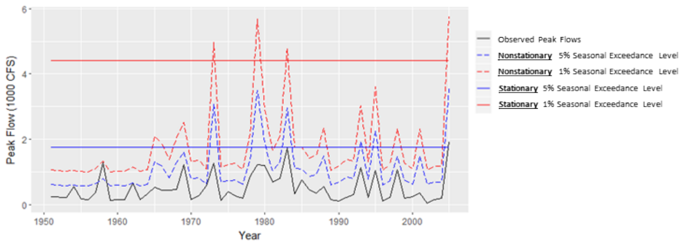

Figure 1 (above): A comparison of historical 5% and 1% stationary GEV and best nonstationary GEV return levels. Gaps represent missing data.

Best Nonstationary GEV Model

Location ~ VIC, Scale ~ VIC

Location		Scale					
μ_0	μ_1	ϕ_0	ϕ_1	**Shape**	**Nllh**	**AIC**	**BIC**
0.13	1.25	-2.36	1.740	0.27	-13.7	-17.4	-7.3

LR Test Against Stationary GEV Model: **p-value=1.621e-13**

Table 1: Fitted parameter values and skill scores for the best nonstationary GEV model.

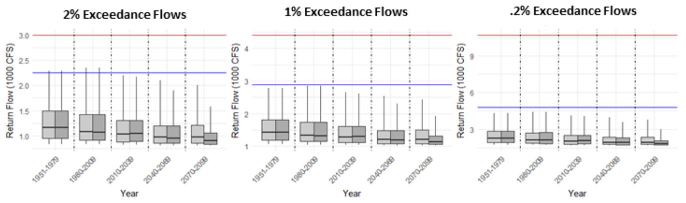

Figure 2 (above): Stationary GEV and LPIII return levels (solid lines) and boxplots of nonstationary return levels generated from the LOCA CMIP5 ensemble of covariates. Results cover two RCP scenarios.

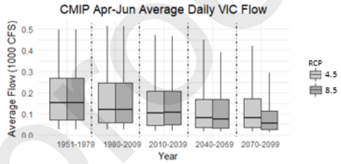

Figure 3 (above): Boxplots of LOCA CMIP5 ensemble covariates. Results cover two RCP scenarios.

Return Flow (1000 CFS)

	Stationary Models		**Nonstationary GEV Model - GCM Ensemble Percentile**									
Exceedance Probability	**GEV**	**LPIII**	**RCP**	**1980-2009**			**2040-2069**			**2070-2099**		
				25th	Median	75th	25th	Median	75th	25th	Median	75th
20%	0.7	0.8	4.5	0.4	0.5	0.7	0.4	0.4	0.6	0.4	0.4	0.6
			8.5	0.4	0.5	0.7	0.4	0.4	0.6	0.3	0.4	0.5
10%	1.2	1.1	4.5	0.5	0.6	0.9	0.5	0.6	0.7	0.5	0.6	0.7
			8.5	0.5	0.6	0.9	0.5	0.5	0.7	0.5	0.5	0.6
4%	2.0	1.7	4.5	0.7	0.9	1.2	0.7	0.8	1.0	0.7	0.8	1.0
			8.5	0.7	0.9	1.2	0.7	0.8	1.0	0.7	0.7	0.8
1%	4.4	2.9	4.5	1.1	1.3	1.7	1.1	1.2	1.5	1.1	1.2	1.5
			8.5	1.1	1.3	1.7	1.1	1.2	1.5	1.1	1.1	1.3

Table 2 (above): Stationary GEV and LPIII return levels and best nonstationary GEV return levels. Percentiles for nonstationary return levels represent the percentile return level from the LOCA CMIP5 ensemble within the specified time period. Results cover two RCP scenarios.

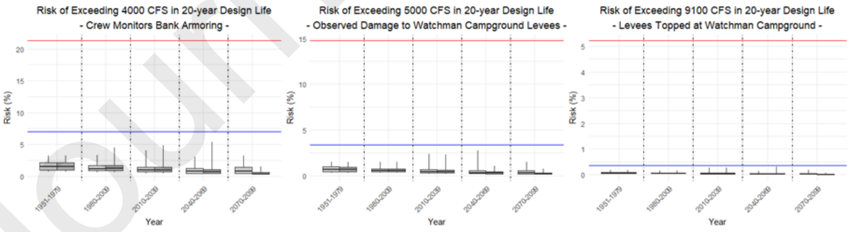

Figure 4 (left): Risk of exceeding critical flows within design life for stationary GEV and LPIII models (solid lines) and best nonstationary GEV model simulations from the LOCA CMIP5 ensemble of covariates (boxplots).

Seasonal Extreme Flow Analysis
Lamar River near Tower Ranger Station, YNP (USGS 06188000)
Yellowstone National Park

Historical Return Levels

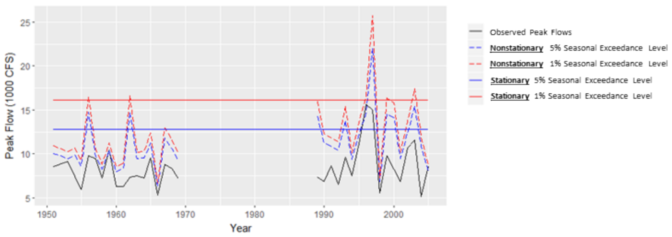

Figure 1 (above): A comparison of historical 5% and 1% stationary GEV and best nonstationary GEV return levels. Gaps represent missing data.

Best Nonstationary GEV Model

Location ~ Pre_VIC+VIC, Scale ~ Pre_VIC+VIC									
Location			**Scale**						
μ_0	μ_1	μ_2	ϕ_0	ϕ_1	ϕ_2	**Shape**	**Nllh**	**AIC**	**BIC**
7.04	-19.72	3.76	-0.06	-7.95	1.52	-0.20	62.1	138.2	149.3

LR Test Against Stationary GEV Model: **p-value=8.761e-06**

Table 1: Fitted parameter values and skill scores for the best nonstationary GEV model.

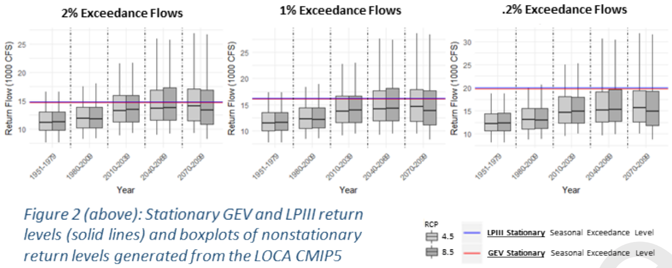

Figure 2 (above): Stationary GEV and LPIII return levels (solid lines) and boxplots of nonstationary return levels generated from the LOCA CMIP5 ensemble of covariates. Results cover two RCP scenarios.

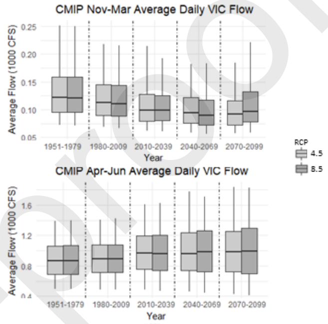

Figure 3 (above): Boxplots of LOCA CMIP5 ensemble covariates. Results cover two RCP scenarios.

Return Flow (1000 CFS)

	Stationary Models		**Nonstationary GEV Model - GCM Ensemble Percentile**									
Exceedance Probability	**GEV**	**LPIII**	**RCP**	**1980-2009**			**2040-2069**			**2070-2099**		
				25th	Median	75th	25th	Median	75th	25th	Median	75th
20%	10.0	10.1	4.5	8.7	9.9	11.2	9.6	11.0	13.1	9.6	11.3	13.2
			8.5	8.7	9.8	11.2	9.7	11.1	13.3	9.1	10.9	13.1
10%	11.4	11.5	4.5	9.2	10.6	12.2	10.3	12.0	14.4	10.3	12.3	14.6
			8.5	9.3	10.5	12.2	10.3	12.1	14.8	9.8	11.8	14.5
4%	13.3	13.3	4.5	9.8	11.4	13.2	11.0	13.0	15.9	11.0	13.4	16.1
			8.5	9.9	11.3	13.2	11.1	13.1	16.3	10.4	12.8	16.0
1%	16.2	16.3	4.5	10.5	12.3	14.4	11.9	14.2	17.7	11.9	14.6	17.9
			8.5	10.6	12.2	14.4	12.0	14.3	18.1	11.2	13.9	17.7

Table 2 (above): Stationary GEV and LPIII return levels and best nonstationary GEV return levels. Percentiles for nonstationary return levels represent the percentile return level from the LOCA CMIP5 ensemble within the specified time period. Results cover two RCP scenarios.

Figure 4 (left): Risk of exceeding critical flows within design life for stationary GEV and LPIII models (solid lines) and best nonstationary GEV model simulations from the LOCA CMIP5 ensemble of covariates (boxplots).

Seasonal Extreme Flow Analysis

Pacific Creek at Moran, WY (USGS 13011500)
Grand Teton National Park

Historical Return Levels

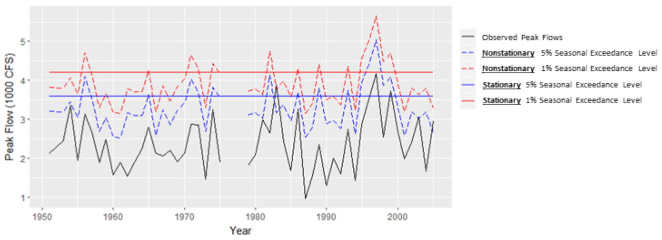

Figure 1 (above): A comparison of historical 5% and 1% stationary GEV and best nonstationary GEV return levels. Gaps represent missing data.

Best Nonstationary GEV Model

Location ~ Pre_Pr + Pr

Location							
μ_0	μ_1	μ_2	**Scale**	**Shape**	**Nllh**	**AIC**	**BIC**
-0.17	0.52	0.29	0.38	-0.004	31.9	73.8	83.5

LR Test Against Stationary GEV Model: **p-value = 4.235e-10**

Table 1: Fitted parameter values and skill scores for the best nonstationary GEV model.

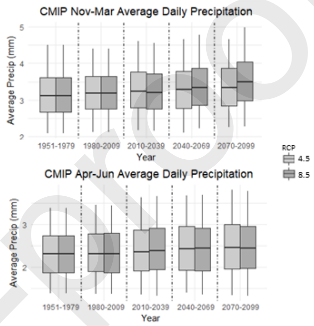

Figure 3 (above): Boxplots of LOCA CMIP5 ensemble covariates. Results cover two RCP scenarios.

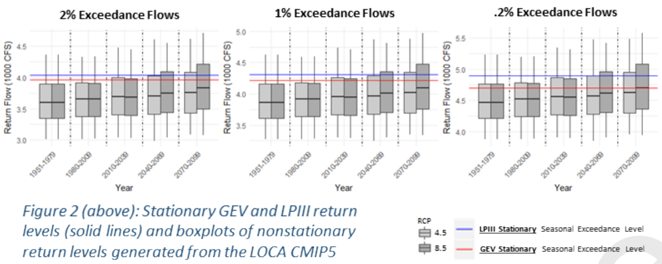

Figure 2 (above): Stationary GEV and LPIII return levels (solid lines) and boxplots of nonstationary return levels generated from the LOCA CMIP5 ensemble of covariates. Results cover two RCP scenarios.

Return Flow (1000 CFS)

	Stationary Models		Nonstationary GEV Model - GCM Ensemble Percentile									
Exceedance Probability	**GEV**	**LPIII**	**RCP**	**1980-2009**			**2040-2069**			**2070-2099**		
				25th	Median	75th	25th	Median	75th	25th	Median	75th
20%	2.9	2.9	4.5	2.5	2.7	3.0	2.5	2.8	3.1	2.5	2.8	3.2
			8.5	2.5	2.7	3.0	2.5	2.8	3.2	2.6	2.9	3.3
10%	3.3	3.3	4.5	2.8	3.0	3.3	2.8	3.1	3.4	2.8	3.1	3.5
			8.5	2.7	3.0	3.3	2.8	3.1	3.5	2.9	3.2	3.6
4%	3.7	3.7	4.5	3.1	3.4	3.7	3.1	3.4	3.8	3.2	3.5	3.8
			8.5	3.1	3.4	3.6	3.2	3.5	3.8	3.2	3.6	3.9
1%	4.2	4.3	4.5	3.6	3.9	4.2	3.7	4.0	4.3	3.7	4.0	4.3
			8.5	3.6	3.9	4.2	3.7	4.0	4.4	3.8	4.1	4.5

Table 2 (above): Stationary GEV and LPIII return levels and best nonstationary GEV return levels. Percentiles for nonstationary return levels represent the percentile return level from the LOCA CMIP5 ensemble within the specified time period. Results cover two RCP scenarios.

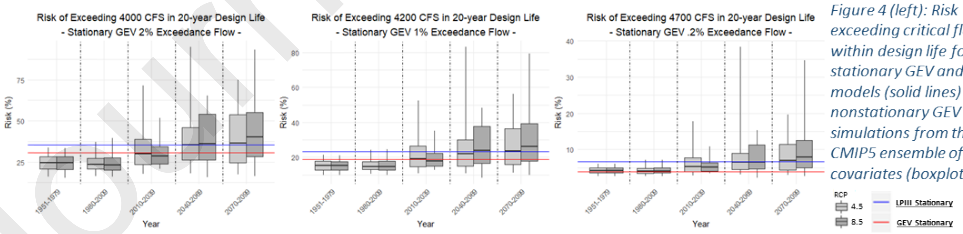

Figure 4 (left): Risk of exceeding critical flows within design life for stationary GEV and LPIII models (solid lines) and best nonstationary GEV model simulations from the LOCA CMIP5 ensemble of covariates (boxplots).

Seasonal Extreme Flow Analysis

Buffalo River near St. Joe, AR (USGS 07056000)
Buffalo National River

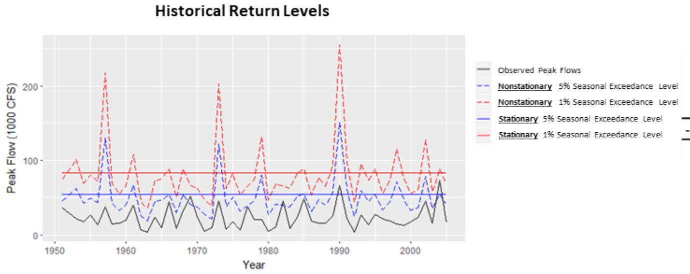

Figure 1 (above): A comparison of historical 5% and 1% stationary GEV and best nonstationary GEV return levels. Gaps represent missing data.

Best Nonstationary GEV Model

Location ~ Pr, Scale ~ Pr							
Location		**Scale**					
μ_0	μ_1	ϕ_0	ϕ_1	**Shape**	**Nllh**	**AIC**	**BIC**
-13.30	8.82	0.55	0.383	0.27	198.4	406.7	416.8
LR Test Against Stationary GEV Model: **p-value=8.373e-10**							

Table 1: Fitted parameter values and skill scores for the best nonstationary GEV model.

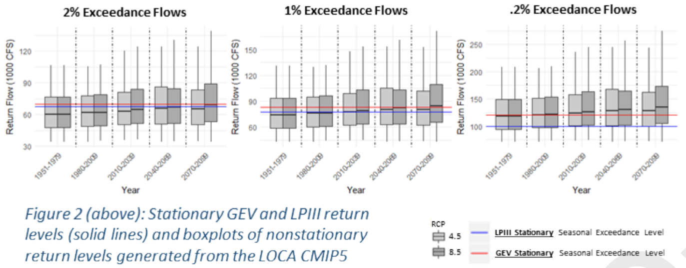

Figure 2 (above): Stationary GEV and LPIII return levels (solid lines) and boxplots of nonstationary return levels generated from the LOCA CMIP5 ensemble of covariates. Results cover two RCP scenarios.

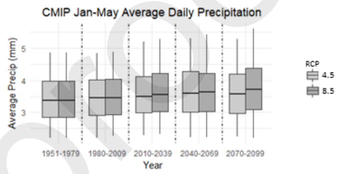

Figure 3 (above): Boxplots of LOCA CMIP5 ensemble covariates. Results cover two RCP scenarios.

Return Flow (1000 CFS)

Exceedance Probability	**Stationary Models**		**Nonstationary GEV Model - GCM Ensemble Percentile**									
	GEV	**LPIII**	**RCP**	**1980-2009**			**2040-2069**			**2070-2099**		
				25th	Median	75th	25th	Median	75th	25th	Median	75th
20%	32.8	34.0	4.5	22.1	29.0	36.9	23.3	31.0	40.9	22.9	30.9	39.6
			8.5	22.3	29.2	37.4	23.5	31.7	40.1	24.5	32.6	42.3
10%	42.9	44.3	4.5	28.7	37.1	46.8	30.1	39.5	52.0	29.6	39.4	50.4
			8.5	28.9	37.2	47.6	30.3	40.4	51.0	31.5	41.6	53.8
4%	57.5	57.6	4.5	39.1	49.9	62.7	40.9	53.1	69.6	40.3	52.9	67.4
			8.5	39.4	50.1	63.7	41.2	54.2	68.3	42.7	55.7	72.0
1%	83.4	77.3	4.5	60.4	75.9	95.0	63.0	80.6	105.4	62.0	80.3	102.1
			8.5	60.8	76.2	96.5	63.4	82.3	103.4	65.5	84.6	109.1

Table 2 (above): Stationary GEV and LPIII return levels and best nonstationary GEV return levels. Percentiles for nonstationary return levels represent the percentile return level from the LOCA CMIP5 ensemble within the specified time period. Results cover two RCP scenarios.

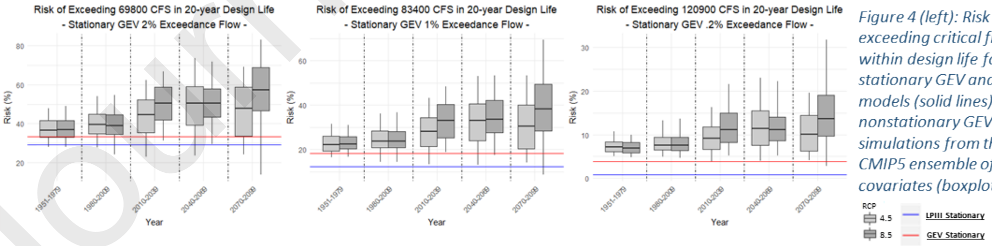

Figure 4 (left): Risk of exceeding critical flows within design life for stationary GEV and LPIII models (solid lines) and best nonstationary GEV model simulations from the LOCA CMIP5 ensemble of covariates (boxplots).

Seasonal Extreme Flow Analysis

Current River at Van Buren, MO (USGS 07067000)
Ozark National Scenic Riverways

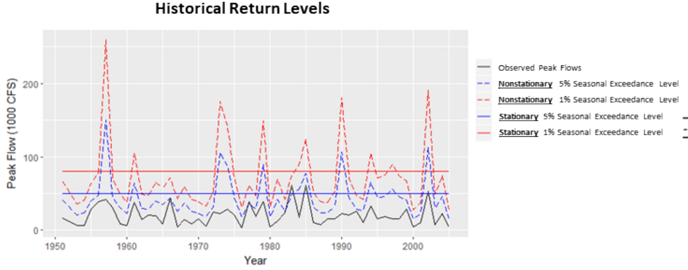

Figure 1 (above): A comparison of historical 5% and 1% stationary GEV and best nonstationary GEV return levels. Gaps represent missing data.

Best Nonstationary GEV Model

Location ~ Pre_VIC+Pr, Scale ~ Pre_VIC+Pr

Location			Scale						
μ_0	μ_1	μ_2	ϕ_0	ϕ_1	ϕ_2	**Shape**	**Nllh**	**AIC**	**BIC**
-17.95	1.32	9.01	-0.22	0.03	0.54	0.27	187.0	387.9	402.0

LR Test Against Stationary GEV Model: **p-value=3.351e-11**

Table 1: Fitted parameter values and skill scores for the best nonstationary GEV model.

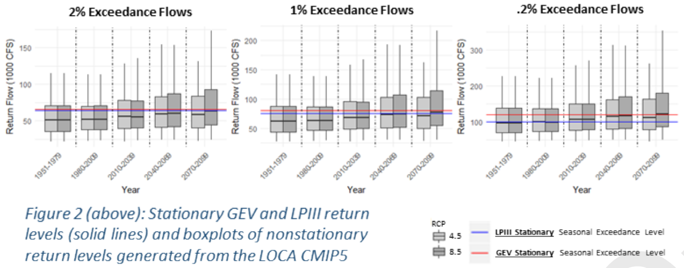

Figure 2 (above): Stationary GEV and LPIII return levels (solid lines) and boxplots of nonstationary return levels generated from the LOCA CMIP5 ensemble of covariates. Results cover two RCP scenarios.

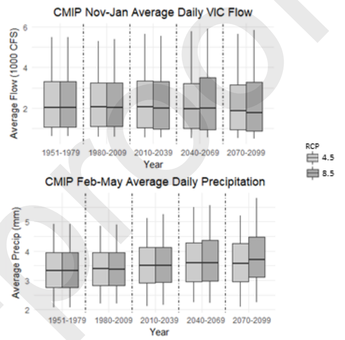

Figure 3 (above): Boxplots of LOCA CMIP5 ensemble covariates. Results cover two RCP scenarios

Return Flow (1000 CFS)

Exceedance Probability	Stationary Models		Nonstationary GEV Model - GCM Ensemble Percentile									
	GEV	**LPIII**	**RCP**	**1980-2009**			**2040-2069**			**2070-2099**		
				25th	Median	75th	25th	Median	75th	25th	Median	75th
20%	29.3	30.3	4.5	17.8	25.3	34.2	19.4	28.7	39.6	19.2	28.2	40.1
			8.5	18.0	25.2	34.2	20.1	29.4	41.3	21.1	30.8	43.8
10%	39.0	40.3	4.5	22.6	31.8	43.1	24.6	36.3	50.4	24.5	35.4	50.8
			8.5	22.7	31.7	43.1	25.5	36.9	52.2	26.8	38.7	55.7
4%	53.5	53.8	4.5	30.4	42.1	57.2	33.1	48.4	67.4	32.9	47.2	68.0
			8.5	30.5	41.9	57.3	33.9	49.0	70.1	36.0	51.5	75.0
1%	80.2	75.1	4.5	46.3	63.5	86.2	50.4	72.8	102.6	49.7	70.9	102.9
			8.5	46.8	63.0	86.4	51.4	73.9	106.9	54.6	77.4	113.7

Table 2 (above): Stationary GEV and LPIII return levels and best nonstationary GEV return levels. Percentiles for nonstationary return levels represent the percentile return level from the LOCA CMIP5 ensemble within the specified time period. Results cover two RCP scenarios.

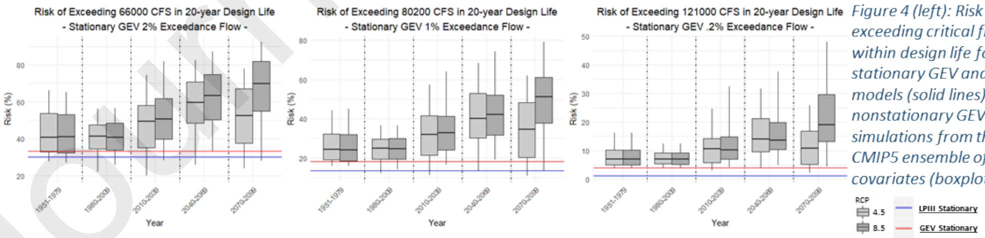

Figure 4 (left): Risk of exceeding critical flows within design life for stationary GEV and LPIII models (solid lines) and best nonstationary GEV model simulations from the LOCA CMIP5 ensemble of covariates (boxplots).

Seasonal Extreme Flow Analysis

Clear Fork near Robbins, TN (USGS 03409500)
Big South Fork National River and Recreation Area

Historical Return Levels

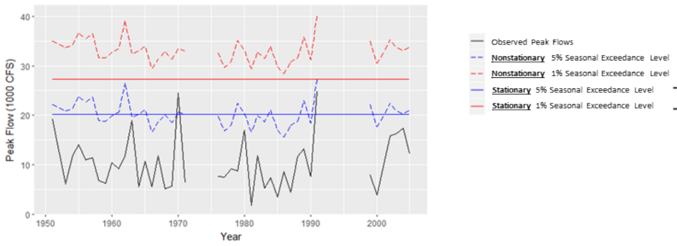

Figure 1 (above): A comparison of historical 5% and 1% stationary GEV and best nonstationary GEV return levels. Gaps represent missing data.

Best Nonstationary GEV Model

Location ~ Pr

Location						
μ_0	μ_1	**Scale**	**Shape**	**Nllh**	**AIC**	**BIC**
-1.87	2.46	2.60	0.29	118.7	245.4	252.6

LR Test Against Stationary GEV Model: **p-value=8.748e-07**

Table 1: Fitted parameter values and skill scores for the best nonstationary GEV model.

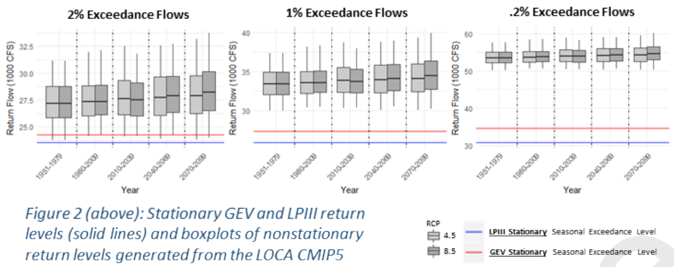

Figure 2 (above): Stationary GEV and LPIII return levels (solid lines) and boxplots of nonstationary return levels generated from the LOCA CMIP5 ensemble of covariates. Results cover two RCP scenarios.

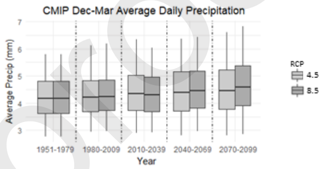

Figure 3 (above): Boxplots of LOCA CMIP5 ensemble covariates. Results cover two RCP scenarios.

Return Flow (1000 CFS)

	Stationary Models		**Nonstationary GEV Model - GCM Ensemble Percentile**									
Exceedance Probability	**GEV**	**LPIII**	**RCP**	**1980-2009**			**2040-2069**			**2070-2099**		
				25th	Median	75th	25th	Median	75th	25th	Median	75th
20%	14.1	14.4	4.5	12.1	13.4	14.9	12.1	13.8	15.7	12.3	14.0	15.9
			8.5	12.2	13.4	14.9	12.4	14.0	15.8	12.6	14.3	16.2
10%	17.2	17.5	4.5	15.4	16.8	18.2	15.5	17.2	19.1	15.7	17.3	19.2
			8.5	15.6	16.8	18.3	15.8	17.3	19.1	16.0	17.7	19.6
4%	21.2	21.0	4.5	20.9	22.2	23.7	20.9	22.6	24.5	21.1	22.8	24.7
			8.5	21.0	22.2	23.7	21.2	22.8	24.6	21.4	23.1	25.1
1%	27.3	25.8	4.5	32.2	33.5	35.0	32.3	34.0	35.8	32.4	34.1	36.0
			8.5	32.3	33.5	35.1	32.5	34.1	35.9	32.7	34.4	36.4

Table 2 (above): Stationary GEV and LPIII return levels and best nonstationary GEV return levels. Percentiles for nonstationary return levels represent the percentile return level from the LOCA CMIP5 ensemble within the specified time period. Results cover two RCP scenarios.

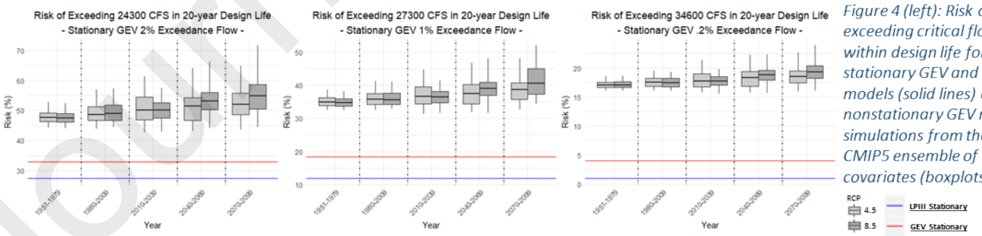

Figure 4 (left): Risk of exceeding critical flows within design life for stationary GEV and LPIII models (solid lines) and best nonstationary GEV model simulations from the LOCA CMIP5 ensemble of covariates (boxplots).

Seasonal Extreme Flow Analysis

Cataloochee Creek near Cataloochee, NC (USGS 03460000)
Great Smoky Mountains National Park

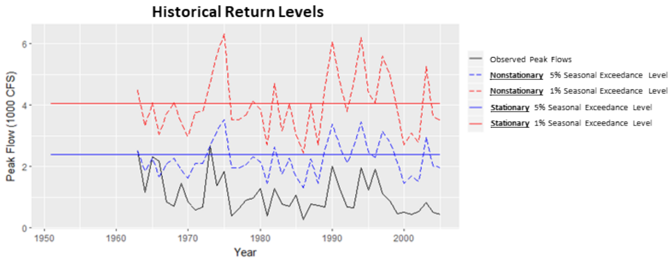

Figure 1 (above): A comparison of historical 5% and 1% stationary GEV and best nonstationary GEV return levels. Gaps represent missing data.

Best Nonstationary GEV Model

Location ~ VIC, Scale ~ VIC							
Location		**Scale**					
μ_0	μ_1	ϕ_0	ϕ_1	**Shape**	**Nllh**	**AIC**	**BIC**
0.14	3.12	-1.94	3.175	0.36	21.7	53.4	62.5
LR Test Against Stationary GEV Model: **p-value=2.034e-05**							

Table 1: Fitted parameter values and skill scores for the best nonstationary GEV model.

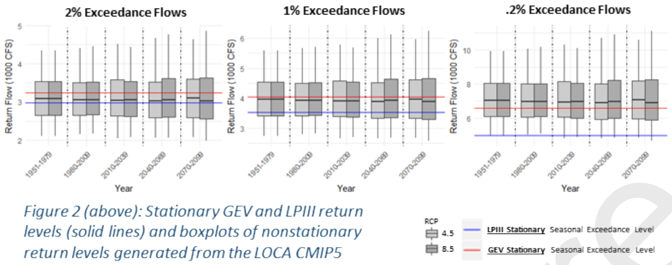

Figure 2 (above): Stationary GEV and LPIII return levels (solid lines) and boxplots of nonstationary return levels generated from the LOCA CMIP5 ensemble of covariates. Results cover two RCP scenarios.

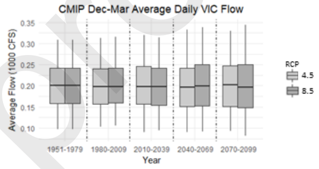

Figure 3 (above): Boxplots of LOCA CMIP5 ensemble covariates. Results cover two RCP scenarios.

Return Flow (1000 CFS)

	Stationary Models		Nonstationary GEV Model - GCM Ensemble Percentile									
Exceedance Probability	**GEV**	**LPIII**	**RCP**	**1980-2009**			**2040-2069**			**2070-2099**		
				25th	Median	75th	25th	Median	75th	25th	Median	75th
20%	1.4	1.4	4.5	1.1	1.3	1.5	1.1	1.3	1.5	1.1	1.3	1.5
			8.5	1.1	1.3	1.5	1.1	1.3	1.5	1.1	1.3	1.6
10%	1.9	1.9	4.5	1.4	1.7	2.0	1.4	1.7	2.0	1.4	1.7	2.0
			8.5	1.5	1.7	2.0	1.4	1.7	2.0	1.4	1.7	2.0
4%	2.6	2.5	4.5	2.0	2.4	2.7	2.0	2.4	2.7	2.0	2.4	2.8
			8.5	2.1	2.4	2.7	2.0	2.4	2.8	2.0	2.4	2.8
1%	4.0	3.5	4.5	3.4	3.9	4.5	3.3	3.9	4.5	3.3	4.0	4.6
			8.5	3.4	3.9	4.5	3.4	3.9	4.6	3.3	3.9	4.6

Table 2 (above): Stationary GEV and LPIII return levels and best nonstationary GEV return levels. Percentiles for nonstationary return levels represent the percentile return level from the LOCA CMIP5 ensemble within the specified time period. Results cover two RCP scenarios.

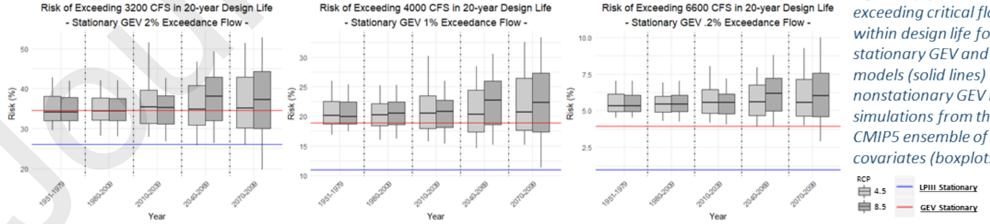

Figure 4 (left): Risk of exceeding critical flows within design life for stationary GEV and LPIII models (solid lines) and best nonstationary GEV model simulations from the LOCA CMIP5 ensemble of covariates (boxplots).

Seasonal Extreme Flow Analysis

Potomac River near Washington, D.C. Little Falls Pump (USGS 01646500)
Chesapeake & Ohio Canal National Historical Park

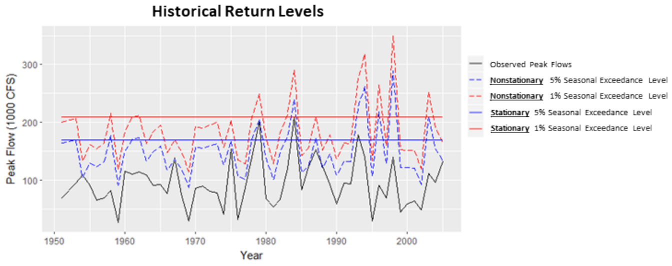

Figure 1 (above): A comparison of historical 5% and 1% stationary GEV and best nonstationary GEV return levels. Gaps represent missing data.

Best Nonstationary GEV Model

Location ~ VIC, Scale ~ VIC

Location		**Scale**					
μ_0	μ_1	ϕ_0	ϕ_1	**Shape**	**Nllh**	**AIC**	**BIC**
-1.87	4.58	2.60	0.029	-0.02	258.7	527.4	537.5

LR Test Against Stationary GEV Model: **p-value=8.749e-10**

Table 1: Fitted parameter values and skill scores for the best nonstationary GEV model.

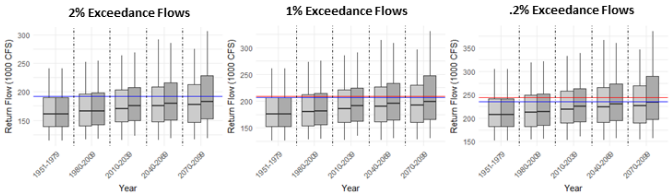

Figure 2 (above): Stationary GEV and LPIII return levels (solid lines) and boxplots of nonstationary return levels generated from the LOCA CMIP5 ensemble of covariates. Results cover two RCP scenarios.

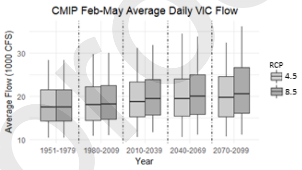

Figure 3 (above): Boxplots of LOCA CMIP5 ensemble covariates. Results cover two RCP scenarios.

Return Flow (1000 CFS)

Exceedance Probability	**Stationary Models**		**Nonstationary GEV Model - GCM Ensemble Percentile**									
	GEV	**LPIII**	**RCP**	**1980-2009**			**2040-2069**			**2070-2099**		
				25th	Median	75th	25th	Median	75th	25th	Median	75th
20%	127.0	129.1	4.5	94.2	114.5	138.0	100.2	121.9	148.2	99.2	123.5	151.0
			8.5	96.0	115.0	139.6	102.4	125.5	153.5	103.9	128.2	163.2
10%	149.1	151.4	4.5	108.9	130.8	156.4	115.3	138.9	167.6	114.2	140.6	170.7
			8.5	110.8	131.4	158.2	117.7	142.8	173.4	119.4	145.7	184.1
4%	174.9	176.2	4.5	127.1	151.1	179.3	134.1	160.0	191.7	132.9	161.8	195.1
			8.5	129.2	151.7	181.2	136.7	164.3	198.2	138.5	167.4	210.0
1%	209.2	206.9	4.5	153.4	180.2	212.2	161.2	190.3	226.3	159.8	192.3	230.2
			8.5	155.7	180.9	214.4	164.1	195.1	233.7	166.1	198.7	247.4

Table 2 (above): Stationary GEV and LPIII return levels and best nonstationary GEV return levels. Percentiles for nonstationary return levels represent the percentile return level from the LOCA CMIP5 ensemble within the specified time period. Results cover two RCP scenarios.

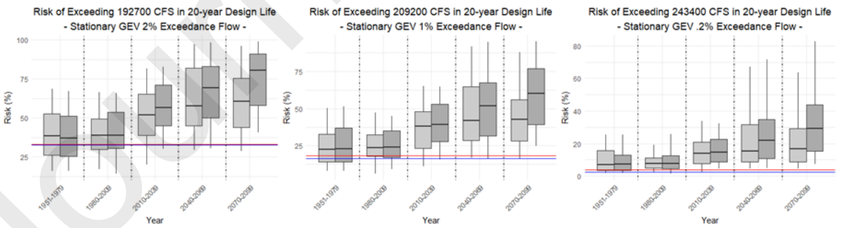

Figure 4 (left): Risk of exceeding critical flows within design life for stationary GEV and LPIII models (solid lines) and best nonstationary GEV model simulations from the LOCA CMIP5 ensemble of covariates (boxplots).

Seasonal Extreme Flow Analysis

Flat Brook near Flatbrookville, NJ (USGS 01440000)
Delaware Water Gap National Recreation Area

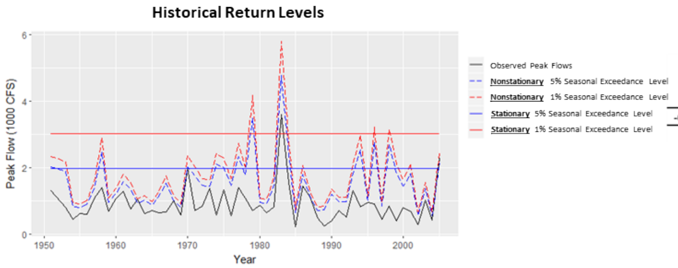

Figure 1 (above): A comparison of historical 5% and 1% stationary GEV and best nonstationary GEV return levels. Gaps represent missing data.

Best Nonstationary GEV Model

Location ~ Pre_VIC+VIC, Scale ~ Pre_VIC+VIC

Location			Scale						
μ_0	μ_1	μ_2	ϕ_0	ϕ_1	ϕ_2	**Shape**	**Nllh**	**AIC**	**BIC**
-0.02	-1.67	6.67	-2.58	-5.12	12.04	-0.22	10.4	34.7	48.8

LR Test Against Stationary GEV Model: **p-value=4.709e-09**

Table 1: Fitted parameter values and skill scores for the best nonstationary GEV model.

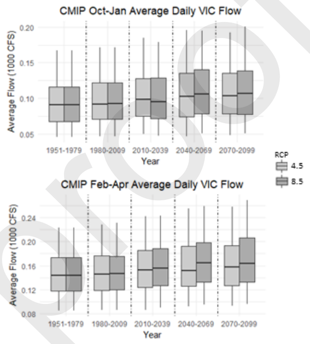

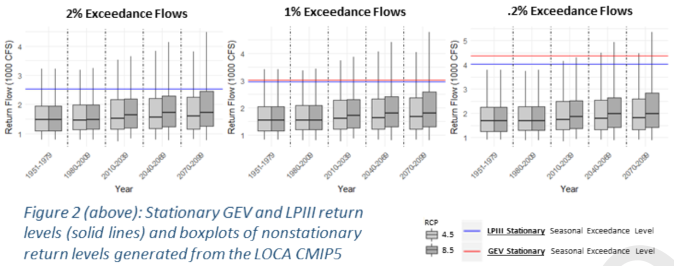

Figure 2 (above): Stationary GEV and LPIII return levels (solid lines) and boxplots of nonstationary return levels generated from the LOCA CMIP5 ensemble of covariates. Results cover two RCP scenarios.

Figure 3 (above): Boxplots of LOCA CMIP5 ensemble covariates. Results cover two RCP scenarios.

Return Flow (1000 CFS)

	Stationary Models		**Nonstationary GEV Model - GCM Ensemble Percentile**									
Exceedance Probability	**GEV**	**LPIII**	**RCP**	**1980-2009**			**2040-2069**			**2070-2099**		
				25th	Median	75th	25th	Median	75th	25th	Median	75th
20%	1.3	1.3	4.5	0.9	1.1	1.5	0.9	1.2	1.6	0.9	1.2	1.7
			8.5	0.9	1.1	1.5	1.0	1.3	1.7	1.0	1.3	1.8
10%	1.6	1.6	4.5	1.0	1.2	1.7	1.0	1.3	1.8	1.0	1.3	1.9
			8.5	1.0	1.3	1.7	1.1	1.5	1.9	1.1	1.5	2.0
4%	2.1	2.1	4.5	1.1	1.4	1.9	1.1	1.5	2.1	1.1	1.5	2.1
			8.5	1.1	1.4	1.9	1.2	1.6	2.2	1.2	1.6	2.3
1%	3.0	3.0	4.5	1.2	1.5	2.1	1.2	1.6	2.3	1.2	1.7	2.4
			8.5	1.2	1.6	2.1	1.3	1.8	2.4	1.3	1.8	2.6

Table 2 (above): Stationary GEV and LPIII return levels and best nonstationary GEV return levels. Percentiles for nonstationary return levels represent the percentile return level from the LOCA CMIP5 ensemble within the specified time period. Results cover two RCP scenarios.

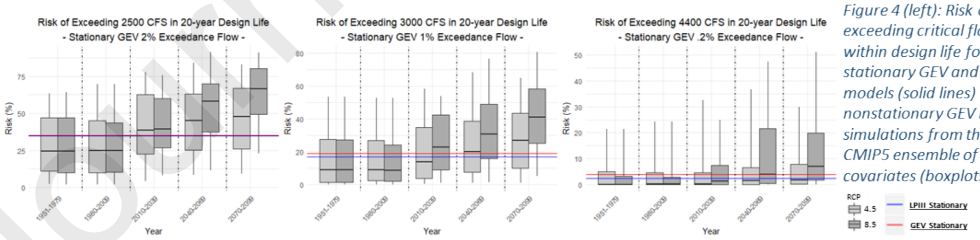

Figure 4 (left): Risk of exceeding critical flows within design life for stationary GEV and LPIII models (solid lines) and best nonstationary GEV model simulations from the LOCA CMIP5 ensemble of covariates (boxplots).

Declarations of interest: none